Appl Phys A (2012) 106:419–446
DOI 10.1007/s00339-011-6690-8

Applied Physics A
Materials Science & Processing

INVITED PAPER

Laser cleaning in conservation of stone, metal, and painted artifacts: state of the art and new insights on the use of the Nd:YAG lasers

S. Siano · J. Agresti · I. Cacciari · D. Ciofini · M. Mascalchi · I. Osticioli · A.A. Mencaglia

Received: 5 April 2011 / Accepted: 7 November 2011 / Published online: 24 November 2011

Abstract In the present work the application of laser cleaning in the conservation of cultural assets is reviewed and some further developments on the interpretation of the associated laser-material interaction regimes are reported. Both the state of the art and new insights mainly focus on systematic approaches addressed to the solution of representative cleaning problems, including stone and metal artifacts along with wall and easel paintings. The innovative part is entirely dedicated to the extension of the application perspective of the Nd:YAG lasers by exploiting the significant versatility provided by their different pulse durations. Besides extensively discussing the specific conservation and physical problems involved in stone and metal cleaning, a significant effort was also made to explore the application potential for wall and easel paintings. The study of the latter was confined to preliminary irradiation tests carried out on prepared samples. We characterized the ablation phenomenology, optical properties, and photomechanical generation associated with the irradiation of optically absorbing varnishes using pulse durations of 10 and 120 ns. Further results concern the nature of the well-known problem of the yellowish appearance in stone cleaning, removal of biological growths and graffiti from stones, cleaning of bronze and iron artifacts and related aspects of laser conversion of unstable minerals, removal of calcareous stratification from wall paintings, and other features.

S. Siano (✉) · J. Agresti · I. Cacciari · D. Ciofini · M. Mascalchi · I. Osticioli · A.A. Mencaglia
Istituto di Fisica Applicata "Nello Carrara",
Consiglio Nazionale delle Ricerche, Firenze, Italy
e-mail: S.Siano@ifac.cnr.it

1 Introduction

Laser cleaning represents the most important contribution of physics to the conservation of cultural heritage. Despite the pioneering works dating back to the early 1970s, this innovative technique started to be systematically investigated and then extensively applied only 20 years later. A number of scientific investigations were reported over the last two decades in journals, conference proceedings, and books, focusing on the efficiency, selectivity, and then effectiveness of laser ablation, as well as on the possible advantages it can provide with respect to traditional cleaning techniques. This triggered an early level of dissemination of the laser approach in conservation practice.

At least 300 Nd:YAG laser systems are presently operative in conservation laboratories and restoration yards all over Europe and abroad. At the same time, laser technologies for conservation also increased their presence in exhibitions and fairs, as well as in formation and tutorial frameworks. Moreover, case studies of important masterpieces also stimulated the interest of mass media, which gave a big resonance to the present innovation, thus extending its dissemination up to the social level.

All this is concrete evidence that laser cleaning technologies moved from research laboratories, to commercial production, and then to restoration yards. Such a unique case of technological and methodological transfer in conservation of cultural assets was entirely determined by the scientific contribution provided by various research institutions. The latter can still play an important role in order to rigorously extend the exploitation of experimental results already demonstrated and address open cleaning problems, thus making durable the methodological revolution the laser approach is producing in conservation practice.

First of all, systematic studies dedicated to the ablation phenomenology and interpretation of the basic laser-material interaction mechanisms are still needed in order to develop practicable solutions for cleaning of wall and easel paintings. At the same time, further insights in stone and metal cleaning can be helpful in order to extend the domain of application.

From a disciplinary point of view, the present application is suffering from lack of thorough physical studies similar to those carried out along the last decades for optimizing biomedical and industrial applications of laser ablation. The results of the latter represent the starting point for interpreting the ablation processes involved in laser cleaning of cultural assets, but exhaustive descriptions must also take into account a number of peculiar features not encountered elsewhere. The variety of ablation channels involved is indeed the widest, according to the different material stratifications, multiplicity of possible degree of cleaning and aims of the laser treatments, which makes the physical approach extremely complex. On the other hand, objective technological and methodological choices should be based on the interpretation of the interaction dynamics other than on phenomenological characterizations.

In the present work, we overview the state of the art of laser cleaning of stone and metal artifacts, along with wall and easel paintings and for each of these conservation topics, the results of new experimental insights are also reported. The latter concern both phenomenological and physical features of the ablation processes involved, which were investigated on sets of prepared samples and artifacts of interest.

The following four sections dedicated to the different conservation problems are organized in a similar way by including an introductory picture presenting the state of the art for the specific class of artifacts, and we present subsections where new original results are presented and discussed. Among the latter, we report for the first time our studies on the use of laser induced plasma spectroscopy (LIPS) and Raman spectroscopy for assessing the cleaning results and on the potential of Nd:YAG(1064 nm) for cleaning wall and easel paintings. The latter was approached through systematic investigations concerning the phenomenology along with aspects of optical properties and ablation dynamics. Thus in particular, significant efforts were devoted to the measurement of the photomechanical effects and to their interpretation, which are presented in a dedicated section providing fundamental information on the basic ablation mechanisms.

2 Stone artifacts

After the mentioned introduction in early 1970s [1–4], laser cleaning was widely applied in stone artifacts restoration works since the second half of 1980s in Italy [5, 6], France [7–13], England [14–16], Portugal [17], Austria [18, 19] and in other countries. Case studies mainly concerned the well-known problem of black crusts produced by urban pollution, but some of them also included the removal of intentional layers applied in the past, even though the latter were not exhaustively interpreted in early investigations.

Extensive applications in conservation works were preceded and accompanied by a number of basic studies carried out in several research projects, which included phenomenological characterizations of irradiation effects, diagnostics of the material removal processes through online measurements and physical modeling [16, 20–34]. Many contributions can be found in LACONA's seven proceeding volumes [35–41], books [42, 43], and review papers [44–46], as well as elsewhere.

In general, these basic studies have been important in order to disseminate the present topic within the scientific community and gather the interest of disciplinary domains (physics, chemistry, geology, art history, archaeology, etc.), to raise the sensitivity of the restorers because of the need to optimize the laser treatments, and to propagate the awareness of the significant potential provided by the novel approach.

Effectiveness and productivity of Nd:YAG(1064 nm) laser ablation were thoroughly investigated in many practical applications, which validated the approach and promoted its acceptance in some countries. Laser cleaning was massively applied in restoration works of historical facades [13, 18, 19, 47], stone reliefs [17, 48], ancient archaeological artworks such as the West Frieze of the Parthenon [49], and unique Renaissance masterpieces, such as for examples the San Marco, Profeta Abacuc, and Pulpito by Donatello, San Filippo, Santi Quattro Coronati and Assunta by Nanni di Banco, Fonte Gaia by Jacopo della Quercia, panels of the Campanile by Andrea Pisano, and many other works [6, 50–54].

Most of the discussions, which accompanied the early stage of application on stones concerning possible side effects associated with laser irradiation, gradually reduced along the last decade while the knowledge of the interaction effects increased through systematic phenomenological and process-optimization studies. These allowed defining operative fluence ranges ensuring effective discriminations between stratifications to be removed and the layers underneath to be uncovered, according with the intrinsic parameters of the laser system and lithotypes under treatment.

Furthermore, also the well-known problem of the yellowish appearance associated with Q-Switching (QS) Nd:YAG(1064 nm) cleaning of whitish stones [9, 55, 56], which significantly slowed the spreading of the novel methodology, was thoroughly investigated [45, 57–60] and mostly solved. In some detail, several studies pointed out

that such a chromatic appearance is mainly due to incomplete removal of pigmented stratifications and/or penetration of organic substances through the outermost material layers of the artifact. In a number of cases laser sputtering can also play a role in determining the yellowish appearance. In these cases, if needed, the very thin chromatic veiling produced can easily be removed by means of any mild action (water poultices, soft abrasion, and other). However, one important order of problem concerning the analytical assessment in a non-invasive way and preferably in situ of the nature of yellowing is still open. An approach based on portable LIPS and Raman spectroscopy is proposed in the following.

Apart from the case of deep penetration of altered oily substances, yellowish appearance can be effectively addressed using suitable laser parameters. Thus in particular, it was demonstrated that Short Free Running (SFR) laser, 20–150 μs [28, 52, 60, 61] and double wavelength QS Nd:YAG laser treatments, including simultaneous 1064 + 355 nm [62–64], and 1064 nm followed by 532 nm [54] often allow to control the final chromatic hue of the stone surface uncovered. Anyway, since also different interpretations of the nature of yellow appearance were reported [65] and the present feature is still an obstacle for laser cleaning techniques in some countries, as mentioned above, further experimental insights were carried out in the present work (see below).

The solution of invasiveness and appearance problems has proven that laser ablation represents the best cleaning methodology for addressing a large variety of conservation problems concerning whitish marble, limestone, and sandstone artifacts. Some case studies concerning laser cleaning of plasters were also reported [66] but extensive applications are still missing.

Laser ablation provides significant advantages with respect to mechanical and chemical approaches in terms of gradualness, selectivity, self termination, and repeatability of the material removal process, as well as in terms of environmental impact. This holds mainly for removing black crusts and intentional layers applied in previous restoration works, such as limewashes (whitewashes), pigmented scialbaturas, oleo-resinous patinations, protective polymeric films, and other. The removal of stratifications from stones can often be achieved using standalone laser treatments, but there are a number of cases where their combination with other techniques may be needed or preferable.

The potential of laser ablation for removing graffiti from stones [67, 68] and for restoring pigmented sandstones have also been investigated [24, 69], even though extensive applications are still missing. Furthermore, in general, also the laser treatment of polychrome stones has to be considered still open. Thus in particular, several works by Spanish research groups explored the capability of laser in order to remove protective layers (i.e. polymers, wax etc.) from granite decorative elements, which pointed out the occurrence of serious discoloration and microstructural damages [70, 71], which apparently do not allow foreseeing a practical application perspective.

Finally, one more stone conservation problem, which needs further efforts, concerns the removal and the inhibition of biological growths (biodeterioration). Let us present the topic in some detail.

The use of laser irradiation for controlled removal of biodeteriogens from stone surfaces was investigated in a few works [72–74]. Studies also included *in vitro* irradiation test on a variety of biological growths [75]. Laser cleaning resulted to be in some cases harmful for the stone substrate because of the high operative fluences needed for removing organic materials strongly anchored to the substrate.

Experiments were performed using excimer [73, 75] and Er:YAG [74] lasers, since aromatic and aliphatic and OH chemical groups exhibit a high optical absorption to the corresponding emission wavelengths.

The laser treatment of lichens using Free Running (FR) Er:YAG(2.94 μm) provided interesting results in terms of thermal deactivation, since the complete destruction of the cellular structure was observed. On the other hand, limitations are due to the low ablation efficiency of this laser.

J.F. Asmus has also proposed to use UV-VIS light of a xenon lamp for the removal of lichens from fragile marble statues. Apparently, effective results were achieved [72] but the lack of thorough diagnostic assessments in order to evaluate the degree of cleaning, deactivation, and durability of the treatment does not allow any conclusive consideration. The possibility to use flash lamps emitting around 100 J/pulse or more is certainly interesting, especially if this can allow an increase of productivity. However, such a vaporization-mediated ablation cannot represent a general solution because of its scarce efficiency, long thermal gradients with high associated average temperatures. Conversely, the flash lamp approach remains very interesting as a potential biocide treatment.

2.1 Pulsewidth-dependence of the ablation rate in stone cleaning

We recently reported descriptions of the Nd:YAG laser ablation processes involved in stone cleaning as a function of the pulse duration [45, 60]. These results are briefly summarized hereafter and organically discussed along with the data collected in further investigations.

A set of prepared samples of black crust (60% gypsum, 30% quartz powder, 8% carbon black, and 2% burnt sienna) on sandstone substrates were characterized through stratigraphic examinations, measurement of reflectance, estimation of the *effective optical penetration depth*, δ, and then subjected to water-assisted ablation tests using QS (6 ns), LQS (Long Q-Switching), and SFR (40–155 μs) Nd:YAG(1064 nm) laser systems.

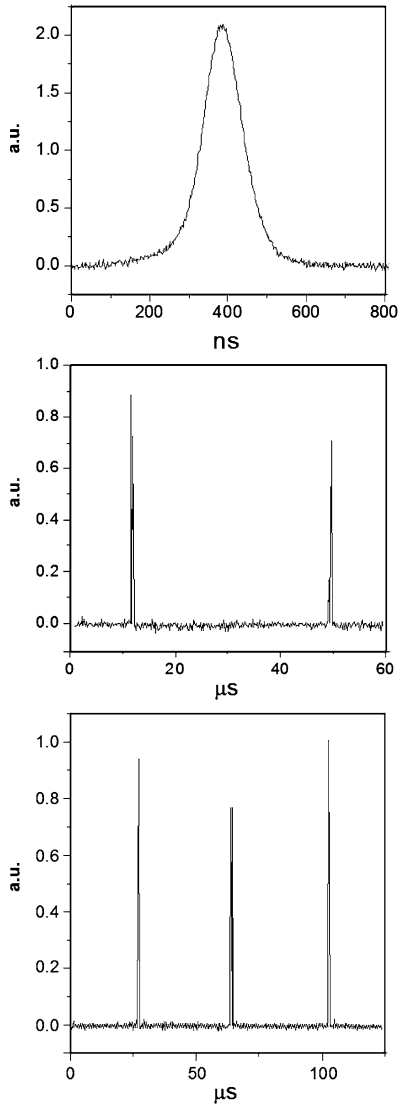

Fig. 1 Temporal profiles of single, double and triple peaks LQS Nd:YAG(1064 nm) laser pulses

The LQS emission was achieved using a laser source equipped with an intracavity optical fiber and a Cr:YAG saturable absorber [76]. Its pulse duration mainly depends on the optical length of the resonator and the reflectivity of the output mirror and can hence easily be changed. Furthermore, the increasing of the pumping energy above the saturation threshold of the absorber also allows the production of laser pulses with multiple peaks (bursts). The single-peak pulses used (LQS_1) had widths of 60 or 120 ns (FWHM) and a constant energy of about 120 mJ. The double (LQS_2) and triple (LQS_3) peak operations provided corresponding rises of the pulse energy (nominally 240 and 360 mJ/pulse, respectively) and had a peak-to-peak temporal spacing of about 40 μs (Fig. 1).

The five different laser emission regimens mentioned above exhibited very different ablative behaviors.

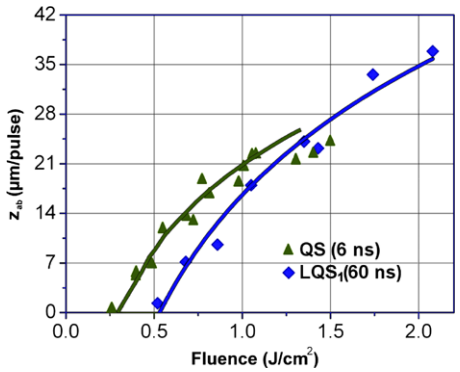

Fig. 2 Ablation rate measurements of black crust (prepared samples) and fittings ($z_{ab} = \delta \cdot \ln F/F_{th}$): comparison between QS and LQS_1 Nd:YAG(1064) lasers

Ablation rates achieved were fitted using the well-known *blow-off* model [77], which assumes that the removal begins above a characteristic fluence threshold $F_{th} = \delta \cdot \varepsilon_{cr}$ (J/cm^2), with ε_{cr} average *critical energy density* (J/cm^3). It provides the following *ablation rate scaling law*: $z_{ab}(F) = \delta \cdot \ln(F/F_{th})$, where the laser fluence F and the fluence threshold F_{th} should be properly referred to the absorption energy flux F_a (radiant exposure) and to the corresponding threshold F_{ath}. However, since $F_a = (1 - R)F$ these irradiation parameters are interchangeable in the previous formula, whereas only the absorption component must be used whenever relating the threshold to temperature rise and critical energy density. In the following, we often use the incident laser fluence F, a parameter which is better suited for defining the *ablative efficiency* as z_{abl}/F.

The saturation of the rate is defined by $z_{ab} = \delta$ occurring at $F = F_s = e \cdot F_{th}$.

This simple model, widely used in laser ablation of biotissues and polymers, provided useful information about the material removal produced by different laser emission regimes.

The analysis of the data pointed out a marked non-linear attenuation of the rate of QS laser against broad linear ablation ranges of LQS_1 and SFR lasers. Despite its saturation rate being lower than the optical penetration depth ($\delta = 16.5$ μm against a measured value of 27 μm), below 1 J/cm^2 the former provided the highest ablative efficiency, whereas at higher fluences the LQS_1 regime was the most efficient (Fig. 2). This feature along with relatively broad operative range (fitting parameters: $F_{th} = 0.56$ J/cm^2, $F_s = 1.51$ J/cm^2, $\delta = 25.8$ μm) and relatively high damage thresholds make the LQS_1 regime of interest for cleaning of whitish stone artifacts. On the other hand, LQS_1 laser cleaning systems presently available on the market emit low pulse energy (150 mJ/pulse against 0.5–1 J/pulse of QS), which makes their *productivity* (m^2/hour) in stone cleaning still not competitive. However, an oscillator-amplifier LQS_1

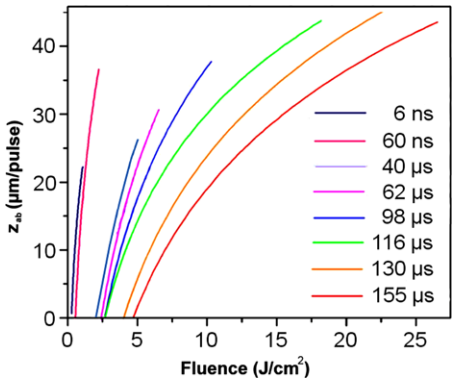

Fig. 3 Ablation rate curves of black crust (prepared samples) using different pulse duration Nd:YAG(1064 nm) lasers: fitting of the experimental data ($z_{ab} = \delta \cdot \ln F/F_{th}$)

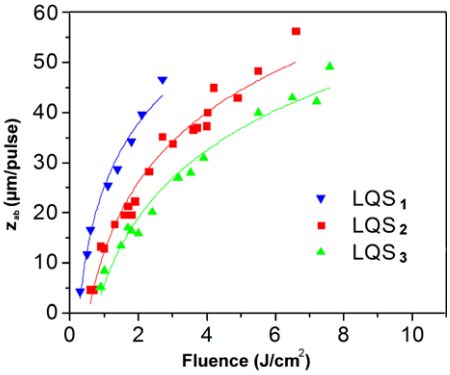

Fig. 4 Ablation rate measurements and fittings of black crust (prepared samples) using single (LQS_1) double (LQS_2), and triple (LQS_3) peak LQS Nd:YAG laser pulses

laser prototype with pulse energy up to 700 mJ/pulse was developed already years ago within collaboration between our group and El.En. S.p.A. (Calenzano, Italy). This system has not been marketed yet, although it represents an interesting technology for high productivity-cleaning of stone artifacts.

The efficiency of the SFR laser emission was decidedly lower than that of QS and LQS_1 lasers: $F_{th} = 2.0$–4.7 J/cm^2, $F_s = 5.9$–12.3 J/cm^2, when $t_L = 40$–150 μs. Figure 3 displays the comparison between ablation rates (fitted curve within the fluence range investigated), which makes evident the strong dependence of the ablation thresholds and rates on pulse duration. Besides the well-known difference between short and long pulses, it is also interesting to note the significant variation within the SFR regime ($F_{th} = 2$–4.7 J/cm^2). The present increase of the threshold is slightly higher than that estimated using a pulse duration dependence $t_L^{1/2}$ (a factor of 2.5 against 2), which derives from the thermal conduction approximation limit: $F_{ath} = \Delta T_c \cdot K_i/2 \cdot (\pi \cdot t_L/D_i)^{1/2}$, where ΔT_c is the *critical temperature rise*, K_i and D_i are the thermal conductivity and diffusivity, respectively, of the present composite insulating material (i.e. the black crust). Such a slightly higher energy loss could be likely due to a shielding effect of the ablated material, which is expected to be more pronounced at longer pulse duration.

Despite the low efficiency, as mentioned above, the use of SFR lasers in stone cleaning significantly grew along the last years mainly thanks to the high pulse energies of the commercial systems (up to 2 J/pulse), very high damage thresholds allowing for broad operative ranges, gradualness, and, in many cases, lack of yellow appearance of the cleaned surface.

Ablation rate studies were extended to the comparison of LQS_1 (120 ns), LQS_2, and LQS_3. As shown in Fig. 4, the efficiency of multiple peaks is decidedly lower than that of single-peak laser pulses but higher than that of SFR of equivalent pulsewidth.

2.2 Effectiveness tests on open problems

As mentioned above, to date, laser ablation has been used mostly in stone cleaning for removing black crusts and coats (scialbaturas and organic-matrix patinations) applied in the past. In other cases, such as the removal of biological growths and graffiti, experimental tests were not followed by extensive practical applications. The main reason can be mostly attributed to the limitations associated with the use of Nd:YAG laser's fundamental wavelength. Despite the substantial differences between acrylic paints and biodeteriogens, such as for example lichens, both of them exhibit low absorption at 1064 nm because of the deep optical penetration and/or high reflectance.

Preliminary cleaning trials we are performing show that the overall approach to graffiti and biodeterioration favors Nd:YAG laser's second harmonic at which most of the undesired layers exhibit a significant absorption. Thus in particular, a fluence as high as several J/cm^2 at 1064 nm did not provide relevant removal effects on a thin film of lichens on white Carrara marble, whereas the second harmonic was much more effective.

The results of some water-assisted laser irradiation tests carried out on a lapidary sample (from the "*Cimitero degli Inglesi*", Florence, XIX century) on which lichens (*Verrucaria nigrescens* and *Caloplaca citrina*), cyanobacteria (Leptolyngbya), and green algae (*Chlorella sp.*) were isolated are displayed Fig. 5. This shows that the only relevant cleaning effects were achieved at 532 nm and 2.94 μm (FR Er:YAG). However, only the former, which starts to be effective around 1.5 J/cm^2, allows foreseeing practicable treatments. FR Er:YAG laser irradiation had a very low efficiency and hence high operative fluences. Furthermore, it produced a sort of smoothing of the marble surface, which is likely due the high optical absorption of the substrate at 2.94 μm. The latter is recognizable in Fig. 5 along with the revitalization effect produced by water assists shown by the intensification of chlorophyll green color hue.

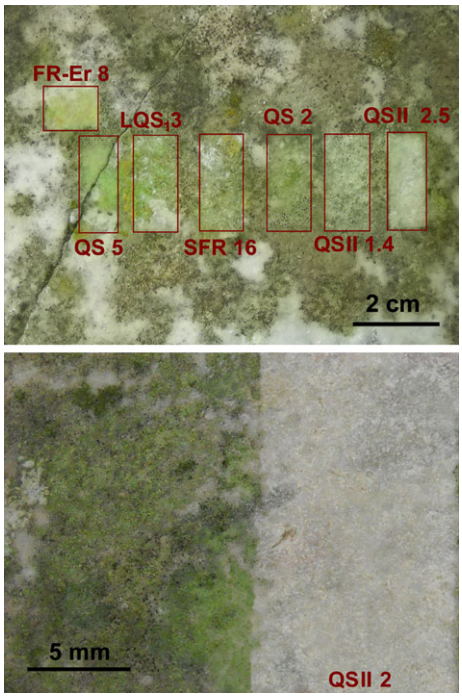

Fig. 5 Laser removal tests of biodeteriogens using different laser wavelength and fluences (indicated in J/cm^2). QSII: 532 nm. FR-Er: 2.94 μm

Laser treatment of biodeterioration at 532 nm requires a rather homogeneous laser spot, since the operative fluence could be only slightly lower than the damage thresholds, which strongly depend on the texture of the surface uncovered. "Fortunately", in a case as that shown in Fig. 5 the whitish marble surface attacked by biological growths is rough and then exhibits high diffuse reflectance and optical penetration, which favor a certain degree of self termination of the removal process. However, no general conclusions are possible since the effectiveness and practicability of the laser cleaning must be evaluated case by case through comparative tests. Moreover, in order to think about a concrete alternative to overall polluting chemical treatments, whenever possible, laser ablation should be preceded by mechanical lightening of the biological growths. This suggestion is an obvious consequence of the relatively low removal efficiency pointed out in the present preliminary tests. It makes no sense in removal of thick biological growths to consider the laser irradiation for preliminary thickness reductions or standalone cleaning treatments.

However, significant insights are needed in order to precisely classify the phenomenology and physical features associated with the Nd:YAG laser treatment of the different biodeteriogens.

Similarly, green wavelength seems to offer the widest versatility in terms of effectiveness and practicability for removing graffiti. It allows to ablate most of the acrylic paint at relatively low operative fluences (the tests of Fig. 6 were

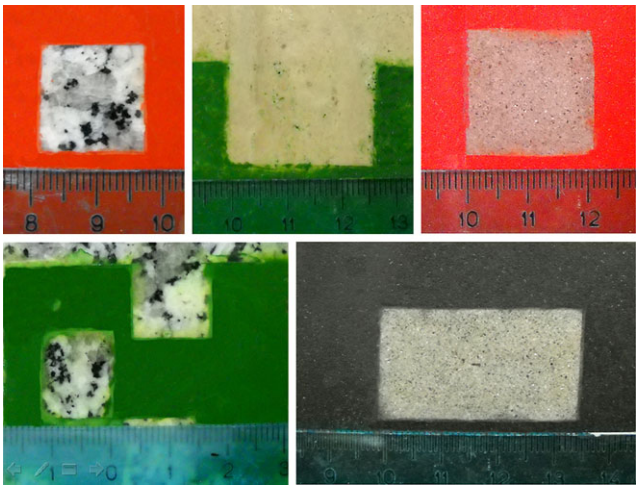

Fig. 6 Removal of graffiti using Nd:YAG laser's second harmonic: operative fluence of about 0.2 J/cm^2

carried out at 0.2 J/cm^2), whereas some problems still remain with metalized varnishes. In any case, laser cleaning can provide a significant contribution in order to address the present problem, as standalone or in combination with low-toxicity chemical agents. Efforts are needed for including the laser methodology within the intervention protocols stated by local conservation institutions.

2.3 Assessing the degree of cleaning and nature of the chromatic appearance

As mentioned above, material removal can be controlled and yellowish appearance of the surface uncovered is prevented in many cases through a suitable selection of laser pulse duration or using the double wavelength approach. On the other hand, the importance of objective characterization of the degree of cleaning and nature of the chromatic appearance during the restoration work should be stressed.

In rigorous approaches, usually cleaning treatments are preliminary defined and assessed through petrographic and compositional analyses carried out on small material samples taken from the artifact. The invasiveness and the complex procedure of this approach strongly limit its overall application. Thus, as a matter of fact, cleaning works are mostly based on naked eye subjective evaluations. Non-invasive characterizations using portable analytical devices should be integrated in the conservation protocol in order to provide prompt answers to a number of interpretation problems, which are usually encountered in the restoration practice. To this goal we evaluated the effectiveness of LIPS and Raman spectroscopy for assessing the degree of cleaning and the nature of the appearance of yellowish after the laser irradiation.

The former was a homemade portable instrument previously described in some details in [78]. Very briefly, we used

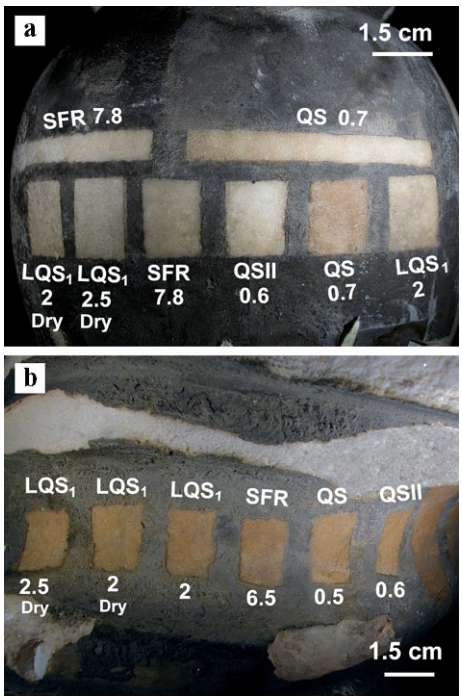

Fig. 7 Comparative cleaning tests of an encrusted baluster (**a**) and a *tortile* column (**b**) using different wavelengths, pulse durations, and fluences. Notations as in Fig. 5. Dry: without water assists (used for all the other tests)

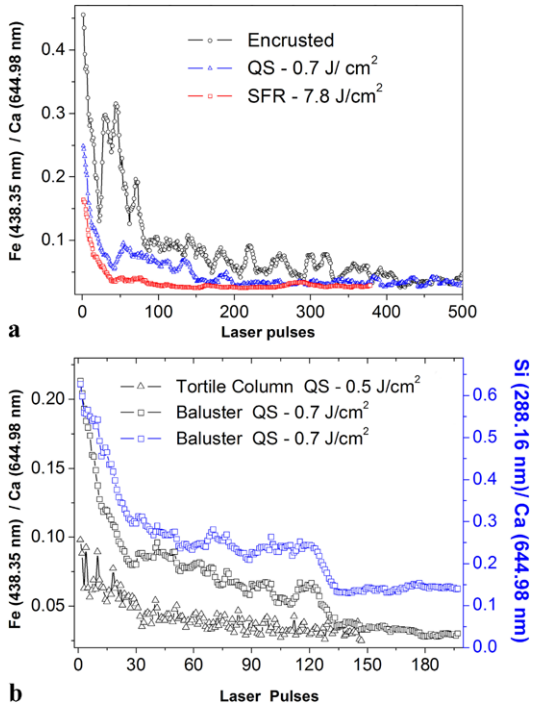

Fig. 8 LIPS Fe-depth profiles of different zones of the baluster (**a**) and tortile column (**b**) uncovered using different laser parameters (see Fig. 7)

a Q-Switched Nd:YAG(1064 nm) and six high resolution Czerny-Turner spectrometers (2,400 grooves/mm) equipped with CCD linear array detectors, which covered the spectral range between 200–890 nm with resolutions ranging between 0.06–0.3 nm. Raman spectra were measured with a compact commercial portable device (3 kg) using an excitation wavelength of 785 nm and a thermooptically cooled detector (2048 pixels). The spectral range and resolution were 260–3200 cm^{-1} and 6 cm^{-1}, respectively.

Laser cleaning tests were carried out on a *tortile* column from Florence's Cathedral and a baluster from the external Loggia of its Dome. Besides microstratigraphic and colorimetric analyses previously reported [60], we measured LIPS elemental depth profiles and Raman spectra in order to understand to which extent these diagnostics can integrate or replace invasive petrographic investigations.

Laser parameters and associated cleaning results are displayed in Fig. 7. As shown, the chromatic hue of the baluster ranged between light orange to white (Fig. 7a), according to the operative conditions, whereas that of the *tortile* column was almost independent of irradiation conditions (Fig. 7b). Figure 8 reports the comparison of Fe(438.35 nm)/Ca(644.98 nm) integrated line intensity ratio measured in encrusted and cleaned areas using QS and SFR Nd:YAG lasers at 0.7 and 7.8 J/cm^2, respectively. As shown, the surface peak of this intensity ratio is relatively intense and broad before cleaning, still significant after QS laser treatment, then less intense and narrow after SFR laser ablation. Furthermore, Fig. 8b shows a clear correlation of Fe/Ca and Si/Ca profiles, thus suggesting the QS laser treatment was incomplete, while SFR laser provided a deeper uncovering. Figure 8b also displays the comparisons between the mentioned yellow site of the baluster with one of the almost chromatically homogeneous sites of *tortile* column. Despite the marked orange appearance of the latter (Fig. 7b), the amplitude of the corresponding iron and silicon depth profiles were relatively moderate. These features suggest a possible organic nature of the present chromatic hue.

Raman spectroscopy, using an excitation source at 785 nm, supported the latter interpretation since the cleaned surfaces exhibited an intense fluorescence, which disappeared at some millimeters beneath the surface (Fig. 9). A similar feature was found for a 19th century plaster from outdoor exposition presenting a thin black crust. The appearance of the yellowish hue after treatment using QS Nd:YAG laser's fundamental wavelength was associated with a significant fluorescence signal, whereas the zone deeply uncovered using the second harmonic was white (Fig. 10).

From previous studies we know some details of the present stratigraphies [60] concerning the presence of a scialbatura on the baluster and a possible organic-matrix patination on the *tortile* column. However, it is particularly interesting from the methodological standpoint to note that the present conclusions were achieved *in situ* without any need to use known microstructural and compositional data.

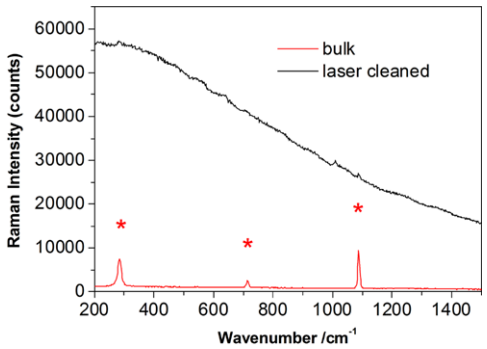

Fig. 9 Raman spectra collected on the *tortile* column (see Fig. 7b) evidencing the significant fluorescence of the laser cleaned area. Red ∗: calcite

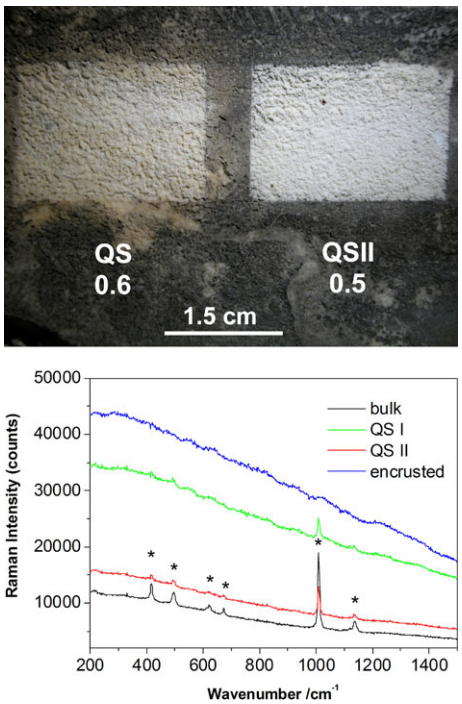

Fig. 10 Cleaning tests performed on an encrusted plaster using 1064 nm (QS) and 532 nm (QSII), at 0.6 and 0.5 J/cm^2, respectively, and corresponding Raman spectra. The gypsum spectrum (∗) was detected only for the latter treatment, whereas the area cleaned with 1064 was fluorescent

3 Metal artifacts

The application of the laser cleaning of metal artworks concretely begun with the case study of the gilded bronze panels of the *Porta del Paradiso* by Lorenzo Ghiberti [79]. This does not mean that Ghiberti's masterpiece was the first metal artifact which underwent laser cleaning tests. Such a fundamental successful example application was preceded by several works on the topic since the early 1990s, including conservation problems of archaeological objects [80, 81], modern sculptures [82], and other [83]. Rather, the *Porta del Paradiso* represents the first case where a critical selection of the optimum laser parameters was operated, which led to the introduction of a novel dedicated laser system called Long Q-Switching (LQS) Nd:YAG(1064 nm) already presented above. It provided an adjustable pulse duration ranging from some tens of nanosecond to some microseconds [76].

The effectiveness and safety of the novel laser temporal regime for cleaning mercury amalgam gilding (experiments were carried out between 30–300 ns and the pulse-length selected for the Door was 70 ns), gold laminas, silver and related alloys were thoroughly demonstrated [79, 84–86]. The case study of Florence's Baptistery East Door disclosed new practical application perspectives and effectively contributed to reduce the skepticism of the conservation community against the laser approach, which was still significant ten years ago.

Overall applications of LQS Nd:YAG laser treatments silver artifacts were reported in 2004 and 2007. The former case was the Treasure from Rimigliano (about 3500 silver alloy Roman coins dated 230–260 a.C.), which was partially cleaned (about 300 coins) using laser ablation in underwater irradiation conditions [45, 87] by exploiting cavitation-mediated processes (see for example [88] and references therein). The latter (2007) represents the first application of laser ablation in order to address the well-known problem of silver tarnishing using Nd:YAG(1064 nm) laser [45, 89]. Metal artifact case studies indeed significantly extended the application domain of laser cleaning that up to 2000 was substantially confined to whitish stone reliefs and statues.

A further fundamental step ahead was represented by the cleaning of mordant (or oil) gilding decorations. The restoration works of the *Santi Quattro Coronati* by Nanni di Banco [90] and of the David by Andrea del Verrocchio [91] demonstrated SFR Nd:YAG lasers represent the best selection for uncovering gold leaf decorations with stratified black crusts and oleo-resinous patinations [92]. The safeguard of gilding as a result were found to be better than that provided by any other technique. After these two successful case studies the recover expectations of similar gilded decorations, which were suspected to be present also on other Renaissance masterpieces, suddenly increased within the conservation community. Laser cleaning was then applied to a number of gilded artworks, such as the San Matteo by Lorenzo Ghiberti [93], the Capitello by Michelozzo, the Amore Attis [94] and the David [95] by Donatello, and other items.

Laser ablation has also been recently used in restoration of large bronze sculptures (not gilded). Case studies included the removal of organic matrix patinations on archaeological bronzes, such as the Etruscan statue named the Arringatore, which is presented in the following, of black crusts from outdoor Mannerist masterpieces, such as Vincenzo Danti's sculptural group the Decollazione del Battista, Baptistery of Florence [96].

Very interestingly, also some modern copper alloy outdoor sculptures underwent laser cleaning treatments, such as the Monument to Lord Nelson in Liverpool and the monument of Queen Victoria in Southport [97].

Finally, several experimentations were carried out on iron objects [81, 98–103] but only a few application case studies were reported [104]. Hereafter, we present some more insights on this topic.

The picture described above shows that laser cleaning of metal artifacts has undergone thorough investigations and has been very successful in several cases of precious metals and bronze artifacts, which could suggest the present domain of application well-established. On the other hand, despite basic studies having been reported by research groups from various countries it is quite evident that most of the applicative work was carried out in Florence, which means there is still a strong need of dissemination.

3.1 Metal surfaces: optimization aspects

The optimization of cleaning of metal objects is mainly based on the evaluation of the thermal aspects whenever the uncovered surface does not exhibit relevant mineralization phenomena. The heating of the uncovered surface must be taken well below the critical temperature. For metal thickness of the order of microns and above, estimations can be achieved roughly considering a thermally insulated metal film of thickness l, subjected to a heat flux corresponding to a homogeneous laser absorption intensity $I_a(t) = (1-R)I(t)$, where R is the reflectance of the metal surface and $I(t)$ the incident laser intensity. The one-dimensional temperature rise in the sheet is described by the following (see [85] and references therein):

$$\Delta T(z,t) = \frac{1}{K_m}\sqrt{\frac{D_m}{\pi}}\left\{\int_0^t I_a(t-t')\frac{e^{-\frac{z^2}{4D_m t'}}}{\sqrt{t'}}dt' + \sum_{n=1}^{\infty}\int_0^t \frac{I_a(t-t')}{\sqrt{t'}}\left[e^{-\frac{(2nl-z)^2}{4D_m t'}} + e^{-\frac{(2nl+z)^2}{4D_m t'}}\right]dt'\right\}, \quad (1)$$

where K_m and D_m are the thermal conductivity and diffusivity of the metal, respectively. $D_m = K_m/(\rho_m C_m)$, with ρ_m and C_m density and specific heat capacity of the metal, respectively.

Conversely, when the thickness is small like that of gold leaf (0.1–0.5 μm), the conduction of the substrate is important even when it is insulating and the following "metal surface layer approximation" can be used [85, 92]:

$$\Delta T(z,t) = \frac{I_a}{bK_i}\left[2b\sqrt{\frac{D_i \cdot t}{\pi}}\cdot e^{-\eta^2} - (1+bz)\operatorname{erfc}\eta + e^{b(z+D_i\cdot b\cdot t)}\operatorname{erfc}\left(\eta+\sqrt{D_i\cdot t}\right)\right], \quad (2)$$

where, as above, the index i indicates an insulating substrate, such as for example glue and minerals, which represents the most typical situation, $\eta = z/2(D_i t)^{1/2}$, $b = r_i C_i/C_{m1}$, with C_{m1} the thermal capacity per unit area of the metal.

Laboratory irradiation tests and associated numerical estimations using (1) allowed demonstrating that for mercury amalgam (fire) gilding, gold laminas, silver, and other precious metal alloys sheets, LQS_1 Nd:YAG(1064) lasers are very effective and in most conservation cases represent the best solution. For fire gilding the pulse duration optimization criterion is provided by the condition $l = l_{th}$ where $l_{th} = 2(D_m \cdot t_L)^{1/2}$ is the *thermal diffusion length*: $t_L = l_{th}^2/4D_m$. Shorter pulses drastically increase the temperature in proximity of the irradiated surface, while longer pulses could be acceptable up until the second term of (1), which quantifies the reflection contribution, and gets predominant with respect to the first one, corresponding to the semi-infinite medium component. Thus for example, it was shown that a constant radiant exposure of 150 mJ/cm^2 (F_a) using pulse duration between 6–100 ns (Gaussian profiles) roughly produces surface temperature rises ranging between about 450–150°C, respectively [84].

Pulse duration longer than about 100 ns does not seem to be convenient for uncovering metal film of the order of a micron since the reduction of the metal heating these involve also corresponds to a significant increase of the cleaning threshold, with consequent risks of massive heating by internal reflections, thermal deformation, and melting of the film. Laser cleaning of a thick metal layer does not involve this limitation; thus also microsecond pulses (SFR) could be effective whenever the ablation efficiency and final appearance can be considered acceptable.

SFR lasers also provided unique results for uncovering gold leaf (mordant or oil gilding) from organic patinations and deposits. Practical observations on laboratory samples were coherent with the temperature estimations achieved using (2). Thus for example, the measured damage threshold of gold leaf glued with silicone were 60 and 291 mJ/cm^2 (F_{ath}) for LQS and SFR, respectively, while the corresponding temperatures were about 1200°C and 500°C.

These general physical laser approaches were demonstrated in several cases of gilding decorating the important masterpieces mentioned above, as well as for several silver artifacts. Conversely, overall applications to copper alloy statues are still rare. Similarly, despite several studies having been reported, also the application to iron objects still remains at the experimental level. Hereafter, we briefly describe the recent restoration work carried out on the Etruscan statue named the Arringatore from Florence's National Museum of Archaeology and report some remarks on laser treatment of iron objects in order to provide further examples of effectiveness.

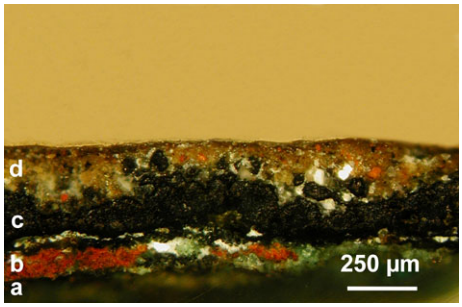

Fig. 11 Representative stratigraphy of the Arringatore including: an organic binder patination (**d**), a black tenorite layer (**c**), corrosion minerals (**b**), and bronze substrate (**a**, missing)

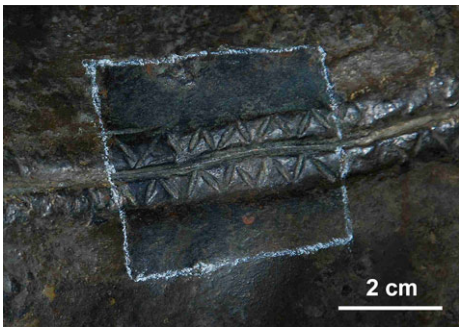

Fig. 12 Laser-assisted cleaning test (laser treatment then scalpel) carried out on the right shoulder of the Arringatore

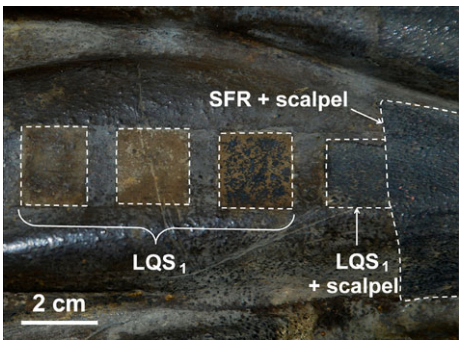

Fig. 13 Comparative laser-assisted cleaning tests carried out on the Arringatore (see the text)

3.2 Mineralized bronze surfaces: the Arringatore and related general implications

The Arringatore is an Etruscan large bronze of uncertain dating between II–I centuries b.C. It is a life-size statue (height: 180 cm) found in XVI century near the Lake Trasimene in Middle Italy and acquired by the Grand Duke Cosimo I in 1566. Supposedly, the statue underwent several undocumented restoration and maintenance works along the centuries.

Thorough investigations were carried out within the recent restoration of this masterpiece in order to collect information on technological features and define the cleaning protocol. Let us focus here on the overall SFR Nd:YAG laser treatment, which was carried out for removing a brown-black patination applied in the past. Here, we also exploit the present example case study for discussing some general aspects of laser treatment of mineralized copper alloy surfaces.

The unwanted patination was an organic-matrix layer of some hundred microns including silicates, calcite, gypsum and a pigment load of carbon black and ochres, along with sporadic presence of Ca- and Cu-oxalates deriving from the mineralization of the binder. This was assessed through several XRD, FT-IR, and stratigraphic analyses.

Figure 11 reports a representative stratigraphy showing from the innermost to the outermost layers: (a) bronze substrate (not visible in Fig. 11); (b) copper minerals, mainly including cuprite and chlorides; (c) an irregular tenorite-rich black layer, also including cerussite, cassiterite, and chlorides; (d) organic-matrix intentional patination; the tenorite layer is a very peculiar feature, which could represent evidence of the original ancient patination. Anyway, apart from this interpretation we will approach elsewhere, the Cu(II) oxide lying on Cu(I) oxide corresponds to the level of the original surface to be uncovered.

Water-assisted SFR Nd:YAG laser irradiation at operative fluencies around 2 J/cm^2 was used to partially ablate and thermally disaggregate the organic-matrix patination; then the cleaning was mechanically finished using scalpel and brush. Such a preliminary treatment was relatively efficient and self-terminated. It was carried out using a pulse repetition rate of 10 Hz and a spot flying time below one second.

Figure 12 displays the final result of a test using such a cleaning procedure. The recovery of the surface readability is evident as well as the tenorite black layer intimately bond to the metal substrate. Tests were also carried out in order to evaluate the possibility of a standalone laser treatment. To this goal LQS Nd:YAG laser was used at fluences between 0.6–1 J/cm^2. However, the uncovered tenorite surface exhibited evident ablation and an undesired appearance (Fig. 13). Even though mechanical finishing and homogenization were apparently satisfactory with a similar appearance as areas cleaned using SFR laser and scalpel, the action of the LQS laser on the tenorite and bronze substrate was judged less controllable or too invasive. Such a choice has a more general valence since, till now, the safe uncovering of black mineralization or black paint layers in wall paintings was possible only using SFR lasers. This is allowed by the low efficiency and large operative fluence range of this temporal regime.

The Arringatore also offered the possibility to apply laser irradiation to remove undesired incoherent copper minerals after mechanical cleaning. This was needed for example for the right arm where a deeper mineralization and lack of the

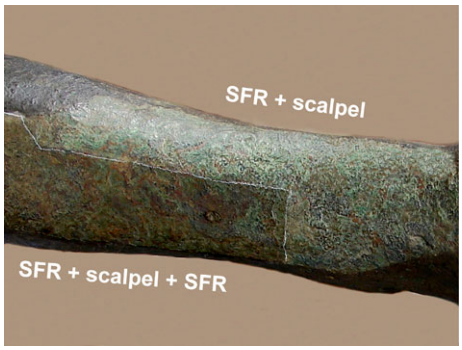

Fig. 14 Arringatore's right arm: comparison between two cleaning treatments with mechanical and laser finishing, respectively

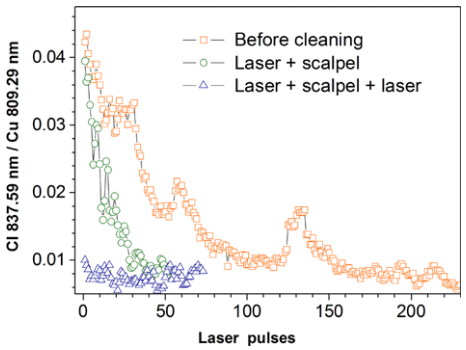

Fig. 15 Chlorine depth profile before and after cleaning in two steps showing significant reduction after laser finishing. The tests were carried out on a corroded Roman lamina

tenorite layer were encountered. As visible in Fig. 14, SFR Nd:YAG laser irradiation at low fluences allowed a deeper degree of cleaning with respect to mechanical finishing and then allowed one to control the final chromatic hue of the surface uncovered. Let us discuss in some more detail this feature.

Systematic irradiation tests allowed demonstrating that SFR laser heating at sufficiently high fluences induces ablation and local phase transformation of unstable copper minerals such as chlorides and carbonates. The chemical reactions of interest are the following:

$$Cu_2(OH)_3Cl \xrightarrow{220^{\circ}C} H_3O^+ + Cl^- + 2CuO, \quad (3)$$

$$2CuCO_3 \cdot Cu(OH)_2 \xrightarrow{180^{\circ}C} 2CuO + Cu_2O + 2H_2O + 2CO_2 + \frac{1}{2}O_2, \quad (4)$$

which foresees phase transformations of chlorides and malachite in tenorite occurring at relatively low temperature. The former (3) suggests that laser irradiation can contribute to contrast the cyclic corrosion of bronze [105] through the removal of chlorine and the formation of stable Cu(II) oxide, thus acting as a passivating treatment. The amount of chlorides transformed, the depth of such transformation, and then the associated surface darkening effect can be controlled through suitable pulse duration and fluence selections. In our experience, this goal is better addressed using microsecond laser pulses at fluencies between about 2–5 J/cm^2. Conversely, nanosecond laser pulses can be useful for ablating incoherent mineral distributions when the metal surface is shielded by relatively deep mineral layers, which can avoid surface micromelting effects. These features are of particular interest in museum maintenance treatments.

In the case of the Arringatore, the final laser treatment in rough and chlorides-rich areas was assessed using LIPS depth profile analysis. A significant reduction of 422.64 nm (superposition of Cl I and Ca II)/458.7 nm (Cu I) line intensity ratio was produced by the final laser irradiation of the surface previously uncovered through SFR laser irradiation and scalpel. Such cleaning, finishing and passivation

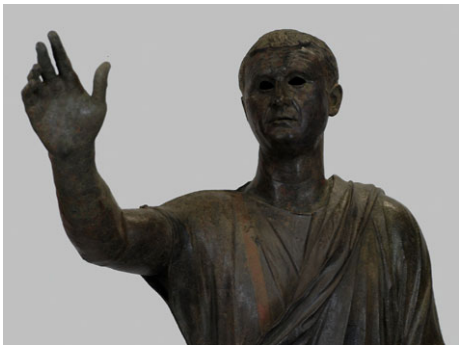

Fig. 16 The bust of the Arringatore after cleaning

effects were also assessed in a more systematic way on a Roman bronze lamina cleaned using SFR laser irradiation and brush 13 years ago, which exhibited a diffused presence of hydroxy-chlorides efflorescence. For this sample the analysis was specifically focused on chlorine by using its isolated line at 837 nm (Cl I) normalized with Cu I line at 809 nm. The passivation effect was confirmed through ten depth profile measurements performed before and after the SFR laser treatment each measured in close proximity (Fig. 15).

The bust of the Arringatore restored is displayed in Fig. 16. It represents a very peculiar case of laser cleaning with a final appearance slightly darker than before cleaning but with a more readable surface and a reduction of corroding agents.

3.3 Ironworks

The laser removal of rust from iron artifacts is a rather safe treatment, which can be carried out using nanosecond or microsecond laser irradiations in dry condition, as for traditional mechanical cleanings. The high critical temperature of iron makes surface micromelting rather more controllable than for copper and precious metals. The application of laser cleaning is simpler with respect to the traditional methodologies based on microsandblasting and brushing since it

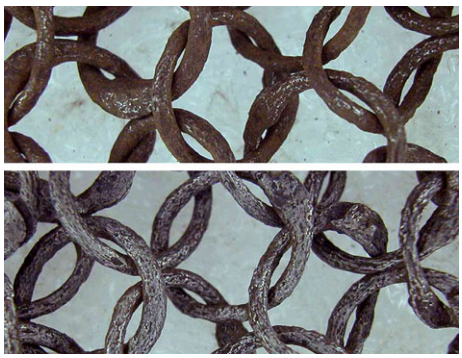

Fig. 17 Protection net of a XVII century helmet: result of the laser treatment (*bottom*). The diameter of the iron ring is about 6 mm

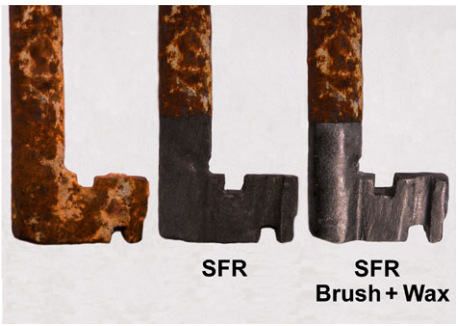

Fig. 18 Example of laser treatment test of a modern iron key

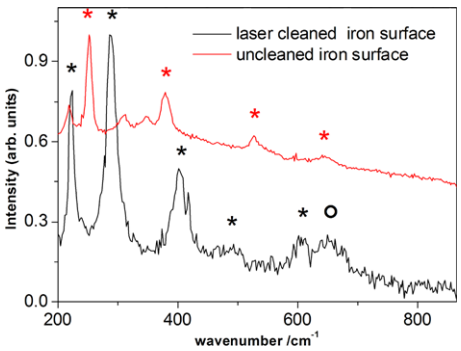

Fig. 19 Rusted iron: Raman spectra of untreated and laser treated areas. Red ∗: lepidocrocite. Black ∗: hematite. Black o: magnetite

does not require any special set up, which allows operating *in situ*.

The main feature of laser treatment of iron artifacts is the drastic darkening of the uncovered surface independently from pulse duration and wavelength. It was observed using SFR [103] and QS Nd:YAG, as well as CO_2 lasers [99]. Examples are reported in Figs. 17, 18 showing tests carried out on the protection net of a XVII century Indian helmet and on a modern key, respectively. After a set of comparative trials, which pointed out the advantages of laser treatment with respect to microsandblasting, the helmet was entirely cleaned using QS Nd:YAG laser irradiation at about 0.7 J/cm^2 [104]. The test on the key represents the case of a deep cleaning and passivation using SFR laser irradiation at several J/cm^2. This was carried out only in order to show the effect of an intensive laser treatment, rather than to propose it as a satisfactory restoration result, which cannot be defined here in a univocal way. Despite the high fluence used, no surface melting phenomena were pointed out through ESEM examinations. These practical tests support the possibility to suitably integrate the laser treatment within the restoration work in place of microsandblasting.

However, a thorough interpretation of the blackening effect is of fundamental interest before promoting the extensive application of laser approach to ancient and modern artifacts. Literature contributions assume the "dehydration" of the rust as responsible process, according to the following reactions [99]:

$$2\ \alpha\text{-FeOOH (goethite) [or } \gamma\text{-FeOOH (lepidocrocite)]} + h\nu \rightarrow \gamma\text{-}Fe_2O_3 \text{ (maghemite)} + H_2O \quad (5)$$

$$6\ \gamma\text{-}Fe_2O_3 \text{ (maghemite)} + h\nu \rightarrow 4\ Fe_3O_4 \text{ (magnetite)} + O_2 \quad (6)$$

After testing X-ray diffractometry, which did not allow detecting phase changes associated with laser irradiation, Raman spectroscopy measurements were performed. Figure 19 shows representative spectra of a heavily corroded Roman sword before and after SFR Nd:YAG laser treatment. Observed bands at 252, 379, 527, 643 (shoulder) cm^{-1}, which characterize the spectrum before cleaning, are ascribed to the vibrational modes of the mineral lepidocrocite, γ-FeOOH, (red*), which rules out the effects of transformation of lepidocrocite in maghemite due to Raman excitation, also reported in literature [106].

In contrast, the spectrum detected after laser cleaning shows characteristic Raman bands of hematite (α-Fe_2O_3) at 224, 287, 404, 492 and 606 cm^{-1} (black*). The band at 650 cm^{-1} is instead ascribable to magnetite (Fe_3O_4) or wustite (FeO) (black°).

The predominance of hematite after laser treatment is compatible with the documented transformation of magnetite, wustite, and maghemite in hematite [106, 107]. Thus, in particular, for magnetite:

$$Fe_3O_4 \xrightarrow{200^\circ C} \gamma\text{-}Fe_2O_3 \xrightarrow{400^\circ C} \alpha\text{-}Fe_2O_3 \quad (7)$$

The band at 650 cm^{-1} could not be ascribed to that of maghemite since the Raman spectrum of the standard shows a band at 680 cm^{-1}, which should disappear completely during the irradiation because of its phase transformation under laser excitation. This band should hence be associated with magnetite, taking into account that a frequency shift of about 10–15 cm^{-1} of the magnetite band at 660–670 cm^{-1}, was observed already at low Raman excitation power [106].

Apart from these phase discrimination details, the transformations detected (lepidocrocite in hematite and magnetite), as well as other possible phase changes of Fe-hydroxides in hematite, magnetite, and/or wustite associated with the pulsed laser heating represents a passivation and stabilization of the metal surface. Incoherent and porous rust layers embed water moisture and pollutants and take them in contact with the metal substrate, thus favoring the continuation of its slow dissolution. Furthermore, the loss of rust through environmental physical actions re-exposes to some extent the metal substrate and accelerates its dissolution mechanism. Laser treatment tests show the formation of a coherent layer of stable oxides, which shields the substrate from water and acid rains attacks thus favoring its long term conservation.

It is worth noting that the present experimentation was carried out on areas of the mentioned Roman sword soon after the laser treatment and after about 14 years, by exploiting laser irradiation tests carried out in 1997 [103]. It is also important to note that no discolorations with respect to the typical dark gray or new formation of rust were observed along such a long period of time.

Laser irradiation of corroded iron artifacts involves ablation, chemical passivation, and structural stabilization. The degree of cleaning, spatial extension of passivation and stabilization and, to some extent, the final chromatic appearance can be controlled by suitably scaling fluence and laser pulse duration. Choices concerning these specific features strongly depend on the type of artifact and restoration philosophy, but indubitably the laser approach can provide similar final appearances as traditional cleaning with addition of chemical-physical effects, which increase the effectiveness and durability of the conservation treatment. These features are of significant interest also for modern objects.

4 Wall paintings

Along the last five years, the effectiveness of the so-called intermediate pulse duration approach, which refers to the use of SFR and LQS Nd:YAG(1064 nm) lasers, was also extensively shown in a set of wall painting conservation works. Once again, we do not refer to the first investigations but rather to those documented rigorous extensive applications, which provided results of general practical value.

The problems approached included the removal of whitewashes, aged Paraloid®, white and black calcareous crusts, which correspond to the case studies of the wall paintings of the *Sagrestia Vecchia* and *Cappella del Manto* in Santa Maria della Scala, Siena [45, 108], donjon of the Castle of Quart [45, 109], double cubicle P of the catacombs of Santa Tecla, Rome [110], and the cubicle named "*dei fornai*" of the catacombs of Domitilla, Rome [111]. The results of these cases of extensive application (i.e. concerning laser treatments carried out on some tens of square meters) were unexpectedly and impressively good. As for other artifacts, SFR and LQS laser regimes significantly extended the operative fluence ranges with respect to QS lasers, thus allowing controlled removals and minimized undesired effects. However, preliminary positive results were also documented for QS, which was tested in order to remove various encrustations [112, 113].

At the same time, the effectiveness of Er:YAG lasers has also been reported for a series of wall painting cleaning problems. Tests on laboratory samples and real fragments were reported [114, 115] but extensive applications are still missing.

The thermal sensitivity of pigments represents a main topic of investigation. Tests using QS Nd:YAG(1064 nm) have shown that, in general, iron pigments exhibit the highest alteration thresholds with respect to shorter wavelengths [116]. In the next section we summarize the results of the systematic studies carried out on some iron pigments, which supported the application cases of LQS and SFR Nd:YAG(1064) lasers mentioned above.

4.1 Systematic approach to Nd:YAG(1064) laser cleaning of wall paintings

Samples were prepared according to the *buon fresco*'s technique [117] on ceramic supports (about 10 × 10 cm). The pigments used were: hematite, yellow ochre, red ochre, raw Sienna, and green earth. After some weeks, the pictorial samples were suitably coated having in mind cleaning problems of practical interest by applying: (1) a suspension of carbon black and gypsum in acetone to mime a thin black crust; (2) a thin whitewash layer on the previous black crust, as encountered in real cases; (3) Paraloid B72® mixed with amorphous carbon and gypsum in order to simulate the dark and optically absorbing Paraloid layer encountered in the case study of the Sagrestia Vecchia mentioned above.

In all the cases the main aim of the technical samples prepared in the present work was to simulate to some extent the physical parameters encountered in practical cases, which determine the ablative effects of laser irradiation. These are mainly related with the optical, thermal and mechanical properties of the materials under irradiation. Conversely, the laboratory samples should not be intended here as a simulation of the real deterioration phenomena, which are and will remain very badly replicable in laboratory. Furthermore, it seems also useful to recall that besides helping to describe basic mechanisms, systematic ablation tests on technical samples are mainly exploitable in comparative studies in order to point out the most significant interaction differences associated with different irradiation parameters. This is the basis of the physical approach to the laser cleaning problems.

Irradiation tests were carried out using QS, LQS, and SFR Nd:YAG lasers in dry and water-assisted conditions. In dry conditions discoloration occurred at relatively low fluences, while water assists fully prevented this phenomenon, which was never observed, neither during laboratory tests nor in applications in real cases. Laser discoloration of iron pigments in wall paintings is an easily avoidable effect.

The damage fluence thresholds in water-assisted condition, F_d, for one and 25 laser shots, as determined through micromorphological examinations (optical and ESEM-EDX) and colorimetric measurements, are reported in Table 1 along with the reflectance (R) of the samples. It shows a significant increase of F_d with the pulse duration, up to above 4 J/cm^2, while a relevant reduction was found when increasing the number of laser pulses, which evidenced the occurrence of cumulative effects. The thresholds of QS were too low with respect to the cleaning threshold of the various samples. Table 2 lists the operative ranges in water-assisted conditions, which allowed achieving satisfactory cleaning results.

The most critical and sometime untreatable situation was that with whitewash alone, whereas its removal was strongly simplified when it was in superposition onto the black crust. Whitewash spallation was achieved already at 0.2 J/cm^2 using the LQS laser, almost independently of the pigment. The complete removal of the underlying black crust was achieved already at about 0.3 J/cm^2. However, this case was also treatable using the SFR laser and by combining the two temporal regimes, as clearly shown in Fig. 20. Colorimetric assessments in cleaned areas showed the complete chromatic recover with color differences (ΔE) under the perceptivity threshold of human eye.

It appears (Tables 1, 2) that the operative fluence ranges were rather narrow in some cases. Anyway, similarly to other laboratory simulations, it should be underlined that the main aim of the present experimentation was the comparison among different laser approaches, while the thresholds determined should be considered just as indicative values. As a matter of fact, till now, the damage thresholds encountered in real cases were significantly higher than those of the systematic experimentation. This is reasonable due to the better degree of carbonatization of the real pictorial layer with respect to prepared laboratory samples.

Let us consider for example the case study to the catacombs of Santa Tecla in Rome [110], where laser ablation was extensively used in an entire cubicle in order to remove calcareous crust growths in this hypogean environment. Figure 21 show a typical stratigraphy including calcareous crust (c), an ancient deposit of lump black (p), a red ochre-based pictorial layer (b) and eventually the substrate (lime plaster with sandy aggregate, a). SFR laser allowed the selective removal of the thick calcareous crusts around 3 J/cm^2 (for thick crust) and then of the underlying black crust by rising the fluence up to 5 J/cm^2 (Fig. 21). In this way, it was possible to treat ochre-based painted areas (red and yellow, as well as black pigmented zones using a lower peak fluence (Fig. 22a). In zones where the calcareous crusts were thinner also LQS_1 laser was effective using fluences around 1 J/cm^2 (Fig. 22b). Furthermore, LQS_1 was more effective than SFR for the complete removal of the carbon black layer (p), as is recognizable in Fig. 22b.

During the optimization of this restoration work we also noticed a possible advantage of using multiple pulses (LQS_2, LQS_3), which apparently allowed to reduce the fluence with respect to SFR laser by maintaining similar efficiency and effectiveness. Laboratory tests were carried out in order to investigate this feature.

Table 1 List of frescoed laboratory samples tested, their reflectance at 1064 nm, and damage thresholds

Pigment	R (%)	Laser	Pulses	F_d (J/cm^2)
Hematite	43	SFR	1	2.2
			25	2.0
		LQS	1	1.3
			25	0.6
		QS	1	0.2
Red ochre	72	SFR	1	3.0
			25	2.2
		LQS	1	1.3
			25	0.6
		QS	1	0.2
Yellow ochre	61	SFR	1	3.9
			25	3.0
		LQS	1	1.0
			2	0.94
			25	0.7
		QS	1	0.3
Raw sienna	55	SFR	1	4.0
			25	2.7
		LQS	1	1.0
			2	0.8
			25	0.7
		QS	1	0.3
Green earth	63	SFR	25	3.3
		LQS	1	1.2
			2	1.2
			25	0.9
		QS	1	0.4

Table 2 Operative cleaning ranges of prepared wall painting samples in water-assisted conditions providing satisfactory cleaning results. n.p.: not practicable

Sample	Treatment	SFR	LQS
Hematite	black crust	n.p.	0.4–0.7
	limewash on black	n.p.	0.5–0.6
Yellow ochre	black crust	1.3–3	0.4–0.6
	limewash on black	1.9–2.1	0.4–0.5
Red ochre	black crust	2.0–2.2	0.6–0.7
	limewash on black	2.5–3.0	0.5–0.7
Raw Sienna	black crust	1.3–3.0	0.4–0.6
	limewash on	1.9–2.1	0.4–0.5
Green earth	black crust	2.7	0.5–0.8
	limewash on black	2.0–2.7	0.5–0.7

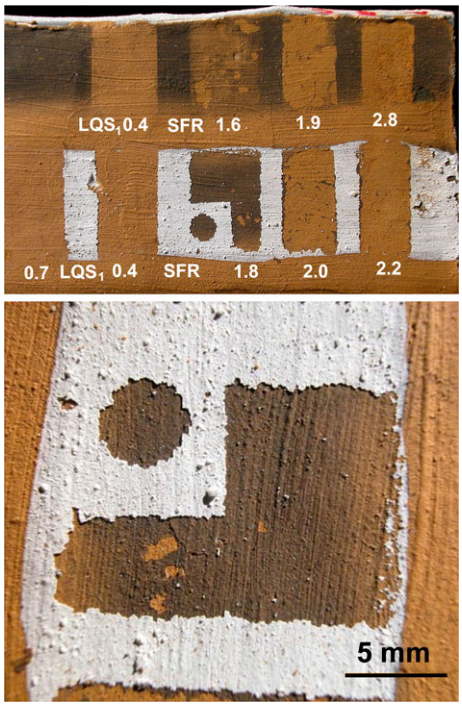

Fig. 20 Selective removal of whitewash and black crust on frescoed laboratory samples

Black crust and whitewashes were applied on aged fresco samples (after two years of preparation). The layer of lime was between 70–200 µm, which induced some variation of the removal thresholds. The histogram of Fig. 23 confirmed the observation suggested by the practical application in the catacombs of Santa Tecla. When using LQS laser pulses with one, two, or three peaks, the increase of the threshold for removing the lime layer was relatively moderate. Thus, the threshold for three peaks was significantly lower than

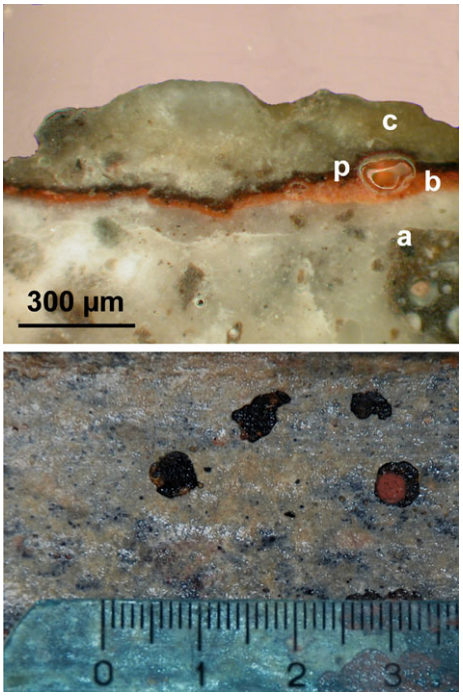

Fig. 21 Paleo-Christian wall paintings of the catacombs of Santa Tecla, Rome. Representative stratigraphy (*top*): (**a**) lime plaster with sandy aggregate; (**b**) pictorial layer; (**p**) carbon black deposit; (**c**) calcareous crust. Single shot cleaning tests (*bottom*): level *p* uncovered at 3 J/cm^2, level *b* uncovered at higher fluence

that of the equivalent length SFR pulse (80 µs). This could be usefully exploited whenever encountering very weak or thermally unstable pictorial layers where the photomechanical and photothermal effects associated with the fluence needed using single-peak LQS_1 or SFR lasers could be invasive. On the basis of this principle, some zones of the paleo-Christian pictorial cycles of the cubicle of Santa Tecla were cleaned using LQS_2 and LQS_3, according to the specific phenomenology.

5 Easel paintings

Easel paintings represent the main challenge of laser cleaning. Despite several works having been reported since the early 1980s [118–120], including systematic investigations on laser interaction effects induced on pigments, binders, and varnishes, as well as some case studies, the laser approach is still far from conservation practice.

Various laser systems were tested, such as excimer lasers emitting at 308, 248, or 193 nm [118, 121–126], Free Running (FR) Er:YAG(2.94 µm) laser [119, 127–129], and QS Nd:YAG(1064, 532, 355, 266 nm) lasers [116, 130–132]. The potential use of the latter was mostly investigated in laboratory tests aimed at assessing the stability of pigments and paint layers under different irradiation conditions.

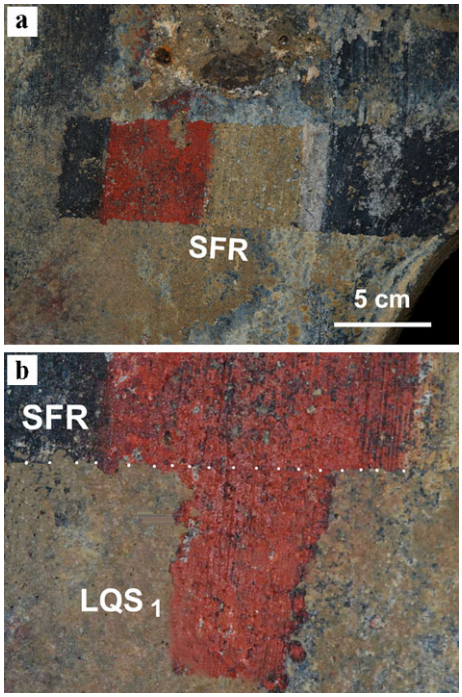

Fig. 22 Paleo-Christian wall paintings of the catacombs of Santa Tecla, Rome: (**a**) effectiveness of SFR Nd:YAG laser on different pigments, (**b**) comparison with LQS_1 laser

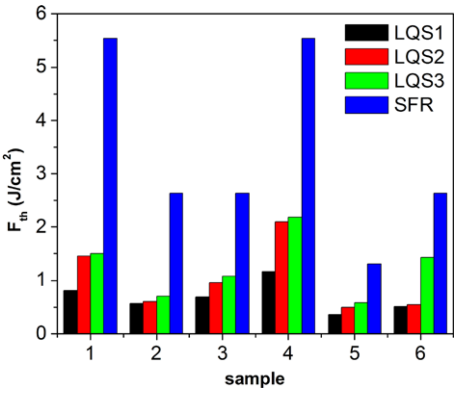

Fig. 23 Comparison among laser spallation thresholds of whitewash on black crust using single (LQS_1), double (LQS_2), and triple (LQS_3) peak LQS Nd:YAG laser pulses

Despite the laser-material interaction mechanisms associated with UV radiation emitted by excimer (or high order harmonics of QS-Nd:YAG) lasers being very different from the ones of the specific near-IR wavelength emitted by Er:YAG laser, their use in the cleaning of painted surfaces has a common feature. In both cases the basic idea is to exploit the very short optical penetration depth (less than 1 μm), which is significantly smaller than the thickness of the layer to be usually removed (aged varnishes, deposits, over-painting etc.). In recent years this approach also brought the proposal of ultrashort lasers in order to minimize undesired side effects.

Studies on the picosecond and femtosecond laser pulses were carried out, which provided promising results [46, 133–136]. The potential of these last generation lasers was investigated using prepared laboratory samples including doped single and multiple polymer layers. The selective removal of the outermost layer was demonstrated also exploiting fluorescence and other optical techniques for monitoring the ablation process [137–140].

As evidenced in various parameterization studies, the direct irradiation of the paint layer by UV radiation produces discoloration and ablation effects occurring at the operative fluences of the laser cleaning [122, 125, 137]. In specific case studies excimer laser irradiation was used for lightening aged varnishes, ablating incoherent deposits at relatively low fluences, and removing over-painting layers under careful monitoring of the uncovering process [125, 141].

Side effects can be minimized when using ultrashort laser pulses. Thus for example, a direct micromorphological change associated with nanosecond and femtosecond UV laser irradiations pointed out that the latter involves reduced alterations with respect to the former [142]. Very interestingly, it was also proved that ultrashort UV laser irradiation (213 nm, 150 ps) can avoid discoloration effects [143]. On the other hand a recent study evidenced the occurrence of cumulative effects when using multiple femtosecond pulses [144].

Experimentations using FR Er:YAG laser pointed out the occurrence of thermal side effects when directly irradiating the paint layer [128]. Problems arise from the lack of thermal confinement due to the long pulse duration (200–400 μs), whose corresponding thermal diffusion length is above one order of magnitude larger than the optical penetration depth in typical materials of interest. Besides the mentioned experimentations [127, 128], systematic tests are still being carried out on canvas and wooden panel paintings for the removal of varnishes, over-painting, black carbon, and animal glue [145].

Within this picture and having in mind all the practical limitations associated with the laser sources proposed to date, we retained our interest to preliminarily test the application perspectives of QS and LQS_1 Nd:YAG(1064 nm) lasers.

5.1 Exploring the potential of Nd:YAG(1064 nm) laser for cleaning easel paintings

About 30 laboratory samples were prepared according to the following procedure: (1) application of gypsum and rabbit glue on wooden panel (15 × 15 cm); (2) application of paint layers using the pure and mixed pigments listed in Table 3; (3) application of a black carbon layer representing an accumulation of deposits or of vanish (dammar or mastic) doped with carbon black.

As mentioned above, we prepared laboratory samples in order to simulate to some extent optical, thermal, and mechanical features encountered in practical situations and carry out comparative evaluations, without facing the difficult task to simulate real deterioration phenomena. In particular, we focused on the removal of dark varnishes often encountered in conservation practice, which can have very different origins. As regards some details, a relevant case is that of the so called pigmented varnishes applied by the authors themselves or by late hands in order to achieve aged appearances. Besides this, deep darkening can also be the result of complex deterioration phenomena including oxidation, deposits, alteration of impurities, and other.

All the irradiation tests were carried out without any liquid assists. The lowest fluences that produced observable alterations to the paint layer after one or ten LQS Nd:YAG laser pulses were carefully determined through microscopy inspections. The main alterations observed were blanching or darkening (linseed binder) effects, which were precursors of ablation of the paint layer observed at higher fluences.

Very surprisingly, single pulse-damage thresholds between 0.8–2.8 J/cm^2 were determined, apart from cinnabar, lead white, and minium, whose sensitivity to laser heating is well-known. The occurrence of damages was strongly dependent on the type of pigment while the influence of the binder was generally less pronounced, but not negligible. The damage threshold significantly decreased for repetitive irradiation (ten pulses), which indicates that the cumulative alteration effects starts at fluences well below those derived by single-pulse tests. Thus, for example, the estimated thresholds of red ochre decreased from 1.2 to 0.7, from 1 to 0.8, and from 0.8–0.4 in egg tempera, fat egg tempera, and linseed oil, respectively. As said, the worst situation was confirmed to be that of lead white, cinnabar, and minium. As well known these pigments exhibit darkening or blackening effects at relatively low fluences. Very interestingly, the damage threshold increased when lead white was mixed with red ochre or lapislazuli (Table 3). However, only the discoloration of cinnabar was permanent, whereas a chromatic recover of lead white and minium was observed in the course of about a week, as also reported in the literature [131].

As for wall paintings, the values of Table 3 should not be intended as absolute, since irradiation trials carried out after several months confirmed that aging produces a general tendency toward a higher resistance of paint layers to the laser irradiation.

Cleaning tests for removing black carbon layers and darkened varnishes were carried out. For most of the samples the possibility of selective partial or complete uncovering was demonstrated (Fig. 24) using the operative fluence ranges indicated in Table 3. The complete cleaning without any observable side effect was achieved also for green earth and lapislazuli mixed with lead white.

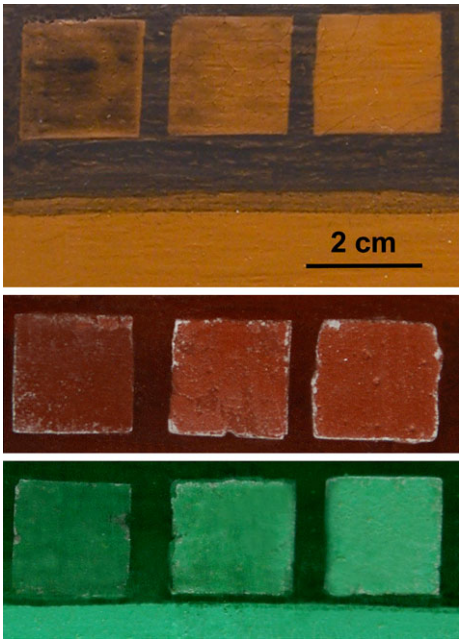

Fig. 24 Evidence of gradual removal on prepared samples of black crust on yellow ochre in egg tempera (**a**) and of doped dammar on red ochre (**b**) and malachite (**c**) in egg tempera, which were achieved using LQS_1 (120 ns) laser

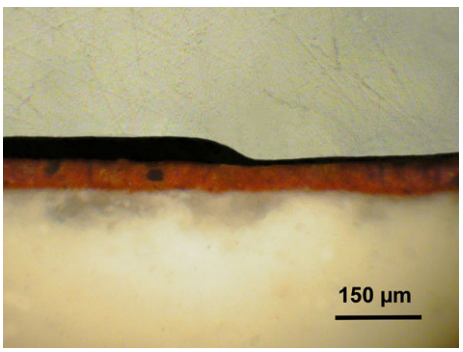

Fig. 25 Cross-section showing the partial removal of doped varnish from red ochre in egg tempera

The uncovered surfaces were characterized through colorimetry and microstratigraphy. An example of partial cleaning of red ochre paint is displayed in Fig. 25. Extensive characterization of laser cleaning phenomenology and of the degree of cleaning allowed proving practicable treatments of the samples with sufficient degrees of self-termination of the ablation processes. The high homogeneity of the energy distribution within the laser spot, which is guaranteed by fiber-coupling of LQS Nd:YAG lasers, was very helpful for achieving the gradual removal.

Table 3 Reflectance, damage thresholds, and cleaning ranges of prepared pictorial samples

Binder	Pigments	*R* (%)	Alteration thresholds		Carbon black	Varnish
			Number of laser pulses			
			1	10		
Egg tempera	*Pure pigment*					
	Yellow ochre	45	1.2	0.7	0.3–0.4	0.2–0.4
	Red ochre	57	1.2	0.7	0.2–0.3	0.2–0.4
	Burnt Sienna	42	1.8	1.2	0.2–0.3	0.2–0.5
	Malachite (light)	20	1.2	0.9	0.2–0.6	0.2–0.5
	Azurite (dark)	50	1.2	0.7	0.2–0.3	0.2–0.5
	Lapislazuli	35	1.1	0.9	0.1–0.3	0.2–0.4
	Cinnabar	67	0.3	n.m.	n.p.	n.p.
	Lead white	65	0.3	n.m.	n.p.	n.p.
	Mixed pigments					
	Verdigris/Yellow Naples (50%–50%)	36	0.95	0.7	0.2–0.3	0.2–0.3
	Green earth/lead white (80%–20%)	39	1.0	0.6	0.2–0.3	0.2–0.3
Fat egg tempera	*Pure pigment*					
	Yellow ochre	64	1	0.4	0.2–0.3	n.m
	Red ochre	n.m.	1	0.8	n.m.	n.m.
	Yellow Naples	86	1	0.3	0.1–0.3	n.m.
	Malachite (light)	23	1.3	0.9	n.m.	n.m.
	Lapislazuli	37	1.6	1.2	0.2–0.3	n.m.
	Burnt Sienna	41	2.7	1.4	0.2–0.3	n.m.
Linseed oil	*Pure pigment*					
	Yellow ochre	60	1.4	0.5	0.2–0.3	0.2–0.3
	Red ochre	74	0.8	0.4	0.2–0.3	0.2–0.4
	Burnt Sienna	36	2.8	1.8	0.2–0.3	0.2–0.5
	Yellow Naples	91	1.2	0.6	0.1–0.3	0.2–0.4
	Cinnabar	61	0.3	n.m.	n.p.	n.p.
	Minium	81	0.5	n.m.	0.1–0.2	0.1
	Mixed pigments					
	Yellow ochre/lead white (80%–20%)	79	0.3	n.m.	n.p.	n.m.
	Red ochre/lead white (80%–20%)	53	0.9	0.2	n.p.	n.m.
	Verdigris/Yellow Naples (50%/50%)	40	1	0.8	0.2–0.3	n.m.
	Lapislazuli/lead white (90%–10%)	38	1.6	0.3	0.1–0.2	n.p.

5.2 Optical aspects of Nd:YAG(1064) laser irradiation of paint layers

The investigation of the potential of laser cleaning of easel paintings using 1064 nm involves irradiation and heating of the paint layer. Besides the precise determination of damage thresholds reported above (Table 3), it is of fundamental importance to estimate the optical penetration and associate heating at the pigment level. To reach this goal, reflectance, transmittance, and scattering measurements were carried on yellow and red ochre, and malachite, in order to achieve preliminary estimations of the optical parameters.

Phase functions $f(\theta)$ and associated anisotropy factor, g, of various pigments were determined through angular energy distribution measurements. Paint layers of the various pigment analysed (yellow ochre, red ochre, and malachite) above 20 μm thickness exhibited an almost isotropic distribution of the transmitted energy, which was satisfactorily fitted with a Rayleigh scattering phase function (Fig. 26):

$$f(\theta) \sim 1 + \text{const} \cdot \cos^2(\theta). \quad (8)$$

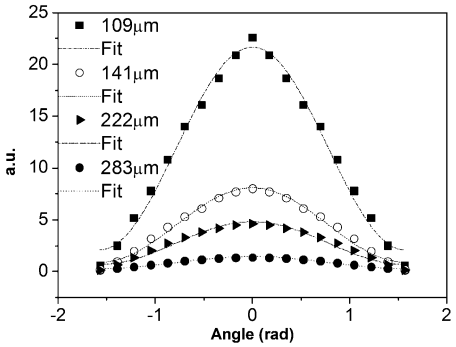

Fig. 26 Scattering phase function of yellow ochre in egg tempera: fitting of the experimental data with a Rayleigh scattering function

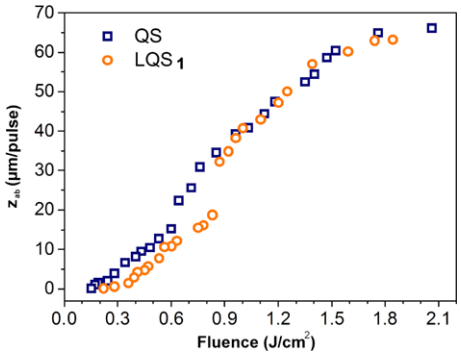

Fig. 27 Ablation rates of doped dammar using QS and LQS_1 Nd:YAG lasers

This allowed us to put $g = 0$ and determine the *scattering* and *absorption coefficients*, μ_s and μ_a, using the theory of fluxes by Kubelka-Munk [146], which provides the Kubelka-Munk scattering and absorption coefficients K and S through the inversion of reflectance and transmittance formulas. In the case of isotropic scattering, as for the present paint layers, K and S are related with the scattering and absorption coefficients μ_s and μ_a through the following expressions [147]:

$$\begin{cases} \mu_a = \eta K, \qquad \mu_s = \chi S, \\ \eta = \frac{(\varphi-1)(1-a)}{\xi(\varphi+1)}, \qquad \chi = -\frac{a(\varphi-1/\varphi)}{2\xi}, \\ \frac{\varphi^2-1}{2\varphi} = \frac{1+R^2-T^2}{2R}, \\ \varphi = \frac{\xi+\ln(1-\xi)}{\xi-\ln(1+\xi)}, \qquad a = \frac{\mu_a}{\mu_a+\mu_s}. \end{cases} \tag{9}$$

In this way the absorption and scattering coefficients, μ_a and μ_s, and hence the effective optical penetration depth δ were derived for the three pigments investigated: $\delta = 97$, 187, 224 μm for malachite, yellow ochre and red ochre, respectively. Such relatively deep penetrations, along with the high reflectances limit the temperature rises under laser irradiation and then broaden the operative fluence ranges for cleaning. Thus for example, maximum temperature rises under an absorption flux of 100 mJ/cm^2 of about 5–9°C, 2–4°C, and 2–4°C can be roughly estimated for the three pigments using $\Delta T(z) = F_a e^{-z/\delta}/\delta C_i$. For this calculation, based on volume-heating, specific heat capacities C_i ranging between 1100–1800 J/kg K were used, which represent the range of variation from epoxy to natural rubber. Similarly, the temperature of the doped dammar used for ablation experiments was estimated to be between 3–6°C/(100 mJ/cm^2).

The results achieved for the other pigments and further aspects of optical properties of pictorial layers will be more extensively discussed elsewhere starting from the methodology described above.

5.3 Nd:YAG(1064 nm) laser ablation rates of absorbing varnishes

As for the removal of black crusts from stones, it is interesting to measure the dependence of the ablation rate of absorbing varnish on the laser fluence and pulse duration. Measurements were carried out on relatively thick samples of dammar homogeneously doped with carbon black producing an optical penetration depth of 147 μm, as estimated through direct measurements and the methodology described in the previous section. The dammar varnish was prepared at 30% in White Spirit (30 g/100 ml, wt/v%), then 1 g of carbon back was added (2.5 wt%).

Ablation tests were carried out on a film of doped dammar with a thickness of about 230 μm on red ochre in egg tempera using LQS_1 and QS Nd:YAG(1064 nm). The ablation depths produced by several laser pulses were measured using a contact-microprofilometer and, as usual, normalized to the single pulse rate. The number of pulses was varied from four (at high fluences) to 100 (limit of the low fluences). The fluence range explored was extended up to 2 J/cm^2.

The results for QS and LQS_1 lasers are reported in Fig. 27. As for black crusts, the former provided a higher efficiency at low fluences, whereas above 0.9 J/cm^2 the rates of the two lasers were practically coincident.

One interesting aspect was the observation of a sort of efficiency jump in the ablation curves around 0.6 and 0.8 J/cm^2 for QS and LQS_1 laser, respectively, which separates two different behaviors. The rate as a result was found to be formerly (low fluences) linear and then exhibited a typical saturating behavior after the mentioned jump, whose possible origin is discussed below.

These features indicate the ablation phenomenology of the two temporal regimens is similar but, at the same time, very different from what observed for black crusts. A fitting with the *blow-off* scaling law would make no sense in this case. Furthermore, for the LQS_1 laser we observed that at a given fluence the first laser shot was significantly more

efficient than the others, whose ablation rate is almost constant. The efficiency jump was much more evident in ablation rates achieved using only the first pulse. This was likely due to the drastic changes of the optical properties of the irradiated surface after the first laser shot, which produces a rather whitish and diffusive appearance. The ablation curve of LQS_1 laser (Fig. 27) should consequently be intended as a quantification of an averaged removal effect, which is of practical interest.

6 Study of the photomechanical aspects of the ablation processes

As reported in several works, photomechanical effects are supposed to play an important role in laser ablation processes involved in laser cleaning of cultural assets. Nevertheless, to date no direct measurements were reported in order to objectively support this assumption and provide some quantitative evaluations of pressure wave involved in the material removal process.

Pressure sensors were realized using 9 μm thick metalized PVDF piezoelectric foils, as shown in Fig. 28. The irradiated sample was the upper component of a sequence of strata including a thin gel layer to ensure the mechanical continuity between the sample itself and the underlying PVDF foil, which is in turn glued to a thick Plexiglas base taking care to avoid the formation of air bubbles. The two metalized sides of the PVDF foil were connected through a short coaxial cable to the high impedance input of the oscilloscope. In this configuration the voltage $V(t)$ is proportional to the pressure $p(t)$ with sensitivity in the order of 1 mV/bar, depending on the area of the pressure front A_p. If the thickness of the sample is much smaller than the area of the laser spot, A_L, a planar approximation can be assumed with $A_p = A_L$. This allows one to derive the following proportionality law: $V(t) = d_{33} \cdot A_L \cdot p(t)/C_{tot}$, where C_{tot} is the total electrical capacitance of the circuit and $d_{33} = 20$ pC/N the piezoelectric coefficient. C_{tot} is practically determined by PVDF foil's capacity (1 nF) that of the cable (20 pF) and of the oscilloscope (10 pF) being practically negligible.

The more systematic pressure transient measurements were carried out for doped dammar slabs with a thickness of 600–700 μm using 10 ns (QS) and 120 ns (LQS_1) laser pulse durations. The irradiation spot was about 2 mm while the fluence was varied between 0.1–2 J/cm^2 using suitable neutral filters. In this condition the attenuation and diffraction of the pressure transient before hitting the PVDF sensor are moderate (see below) and consequently the profile measured is almost coincident with that propagated by laser irradiation in close proximity of the irradiated volume.

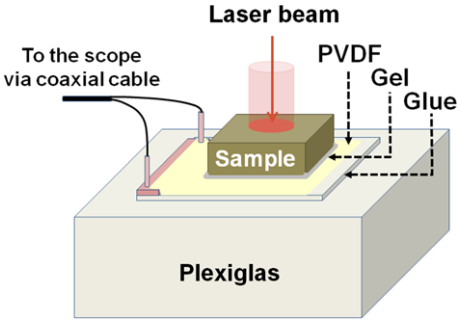

Fig. 28 Setup for measuring pressure transient generated by laser irradiation

The behaviors of the pressure temporal profiles for the two lasers are reported in Fig. 29. At low fluences almost symmetrical double-phase (compression and stretching) pressure profiles were detected, whereas the positive pulse started to be predominant already around 0.2 J/cm^2 for the QS laser, while this threshold was slightly higher for the LQS_1 laser (around 0.4 J/cm^2). Afterwards, the compression phase got much more intense than stretching and its width slightly increased. Without entering the problem of the precise quantification of the pressure peaks, which also requires some consideration on possible reflections occurring before the piezoelectric foil, let us note that pressure peaks of about 225 bar were detected for the QS laser at 1.1 J/cm^2, while the corresponding maximum for LQS_1 was about 97 bar (Fig. 29). These values represent underestimations because of the reflection at the sample-gel interface.

One more interesting feature concerns the width (FWHM) of the positive peak, which was almost constant around 100 ns for the QS and between 155–210 ns for the LQS_1 regime. Finally, the measurements of the pressure wave speed into the dammar bulk provided very variable values, from 1900 to 3000 m/s. This variation showed a dependence on incident fluence and the values measured for QS were higher than for LQS_1 laser.

Very interestingly, a similar behavior as for doped varnish was observed when irradiating a thin slab of prepared black crust with the QS laser (Fig. 30). Differently, the width of the profile was significantly larger, ranging between 200–300 ns when passing from double to single phase with the increasing of the fluence.

The previous features can be interpreted to some extent through the theory of photoacoustic generation.

6.1 Interpretation of the pressure transients and ablation processes

The laser generation of symmetrical double-phase pressure transients as those measured at low fluences (Figs. 29, 30) is theoretically described through the optoacoustic thermoelastic generation theory [148, 149], which can be summarized as follows.

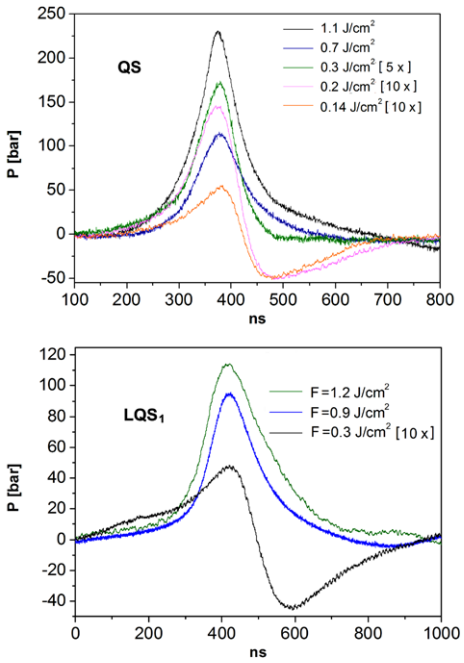

Fig. 29 Behavior of the pressure transient temporal profiles as measured during QS and LQS_1 Nd:YAG laser irradiations of doped dammar at increasing fluences

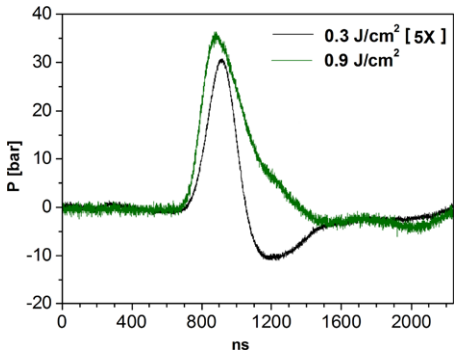

Fig. 30 Pressure profiles measured during QS Nd:YAG laser ablation of black crust

Laser irradiation of an absorbing liquid with pulse duration short enough to realize the thermal confinement condition ($t_L \ll t_{th}$) generates fast thermal transients within the irradiated volume and hence associated pressure rises. This produces a pressure wave, which propagates into the medium with a quasi-sonic speed. This thermoelastic generation is described by the general wave equation:

$$\nabla^2 p - \frac{1}{c^2}\frac{\partial^2 p}{\partial t^2} = -\frac{\beta}{C_p}\frac{\partial \varepsilon}{\partial t}, \tag{10}$$

where c is the sound speed, C_p the specific heat capacity at constant pressure, and β the thermal expansion coefficient of the liquid, while $\varepsilon(x, y, z, t)$ is the laser energy density released into the liquid.

For the present purposes, let us confine the model to the one-dimensional planar case [148, 150], which holds under the condition $d_L/2 \gg \delta$, where d_L is the laser spot diameter. Two different solutions of the propagation equations are determined for rigid (r) and free (f) boundary conditions, respectively:

$$\begin{aligned} p_r(\bar{t}) &= \frac{\beta\delta}{2\pi C_p t_L} \cdot \int_{-\infty}^{+\infty} I_a(t') \cdot \psi(\bar{t} - t')\, dt', \\ p_f(\bar{t}) &= \frac{\delta}{ct_L} \cdot \frac{dp_r(\bar{t})}{d\bar{t}}, \end{aligned} \tag{11}$$

where $t' = t/t_L$, $t' = t_L(t - z/c)$ denotes the reduced time of the co-moving coordinate. ψ is the thermoelastic transfer function for the rigid boundary condition [148, 150]:

$$\psi(\bar{t} - t') = \pi \left(\frac{ct_L}{\delta}\right)^2 e^{-\frac{ct_L}{\delta}(\bar{t} - t')}. \tag{12}$$

The transit time along the distance δ is named *elastic relaxation time*, $t_{el} = \delta/c$. If $t_L < t_{el}$, the pressure into the irradiated volume increases along the whole laser pulse duration since the elastic relaxation occurs at longer times. This defines the *inertial* or *pressure confinement* condition, which gives rise to a high-pressure gradient at the interface. In principle, this condition can be realized when using short pulse duration (e.g. a few nanoseconds) on materials exhibiting relatively large optical penetrations (e.g. several tens of microns).

The compression phase is generated by thermal expansion whereas the development of a rarefaction phase in free boundary condition is due to the propagation and reflection of the compression wave at the solid-air interface. The *acoustical reflection coefficient* is defined as

$$R_{ac} = \frac{Z - Z_0}{Z + Z_0}, \tag{13}$$

where Z_0 and Z are the acoustic impedances of air and liquid, respectively ($Z = \rho c$). Since we have $Z \gg Z_0$, (13) provides $R_{ac} \cong -1$, which corresponds to a total reflection at the water-air interface, which is accompanied by a phase inversion producing the rarefaction peak described by (11).

Despite the whole model above having been developed for absorbing liquids, it can provide useful information also in other situations. Thus, in particular, it has been widely used in the physical diagnostics of laser ablation of soft biotissue [151, 152], which has a predominant water content (70–80%). This is the first time the present theory is experimentally applied in order to investigate the ablation mechanisms in laser cleaning of cultural assets.

6.1.1 *Pressure transients generated in absorbing dammar and associated ablation channels*

In general, let us observe that the thermoelastic optoacoustic model can be used to describe the generation and propa-

gation of the longitudinal pressure transient component assuming that the transverse (or shear) one is negligible or cut away. Without entering into problem of the transverse component in natural resins, let us note that traveling through the coupling gel layer put between the sample and the PVDF sensor (Fig. 28) stops any possible shear component.

On the basis of our previous experiences [152] we can say that apparently the pressure signals of Fig. 29 are not relevantly affected by diffraction effects, as suggested by the presence of single-phase compression peaks. The characterizing parameter of diffraction is given by $D = z/L_D$, where $L_D = d_L^2/4\lambda_{ac}$, with λ_{ac} *acoustic wavelength*. The latter can be achieved from the duration of the compression pulse t_{ac} as measured in close proximity of the pressure source: $\lambda_{ac} = 2t_{ac} \cdot c$. By considering the present pulsewidths and speeds: $\lambda_{ac} = 380$–600 μm for QS and $\lambda_{ac} = 589$–798 μm for LQS_1. Thus, at $z = 600$–700 μm (thickness of doped dammar samples used) $D = 0.2$–0.5, which is allowed, at the present level of discussion, assuming low diffraction effects.

The propagation of pressure transient during QS laser irradiation (sound speed 1900–3000 m/s) corresponds to propagations $z = 19$–30 μm, which is lower than the measured $\delta = 147$ μm or equivalently $t_L < t_{el} = 70$ ns. This means the pressure rise occurs in inertial confinement condition. In this case the acoustic wavelength is determined by the optical penetration depth: $\lambda_{ac} = 2\delta$. The latter can provide an independent estimation of δ in a purely thermoelastic regime. Here, at the lower speed one achieves $\delta = 190$ μm, which could still be considered to be not so different from the measured value. Conversely, at higher speeds such estimation gets incongruent, thus suggesting that overpressure produced by the QS laser has a non-linear origin, i.e. pressure transients are only apparently thermoelastic. This provides a qualitative explanation of the relatively higher photoacoustic conversion efficiency of QS with respect to LQS_1 laser. However, ablation by inertial confinement (i.e. produced by positive overpressure) was not observed, since in this case one would expect a strong reduction of the compression and the lack of the rarefaction phase should be observed at low fluences.

During LQS_1 laser irradiation the pressure wave propagates outside of the irradiated depth ($z = 228$ μm). The acoustic wavelength is hence determined by laser pulse duration, which is roughly in agreement with the measured pulsewidth of the compression peak (155 ns).

For both the lasers, the symmetry of the pressure transient was lost above some hundreds mJ/cm^2. Nevertheless, the compression phase had an almost constant width up to several hundreds of mJ/cm^2. This behavior reveals that the main cause of the material removal has to be attributed to the destructive stretching produced by the negative pressure phase in proximity of the varnish's outer surface. The slight broadening of the compression peak observed for LQS_1 laser at higher fluences could likely be due to the development of a small recoil stress component due to the raising fluid-dynamic contribution.

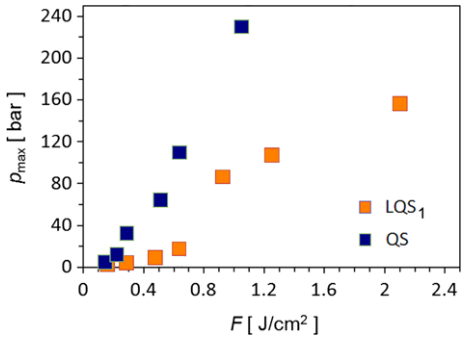

Fig. 31 Dependence of the compression peaks associated with QS and LQS_1 laser irradiations on the fluence

However, spallation is an important component of the ablation process but also the softening of the material and other phenomena seem to be significantly involved. A key of interpretation is suggested by the discontinuity of the ablation rate plots (Fig. 27), which is also observable in the plot of the positive pressure peak as a function of the fluence (Fig. 31). The present efficiency jumps observed at about 0.6 and 0.8 for QS and LQS_1 laser, respectively, have to be associated to the first phase transition of the dammar resin, which is the *glass transition* occurring at a temperature of $T_g = 39$–40°C.

The glass transition is an important phenomenon occurring when heating polymeric materials. Above T_g the energy within the material induces a rotation of the main molecular chain segments, which produce an increase of the free volume of the polymer, and then an increase of the thermal expansion and elastic coefficients. The material does not melt (T_m is much higher than T_g); rather it is softened, even though T_g should not be confused with softening T_s, which refers to the macroscopic softening occurring at higher temperature (for dammar $T_s \cong 90$°C, $T_m \cong 180$°C).

Hence the discontinuities of Figs. 27 and 31 are reasonable due to the glass transition of dammar. Conversely, the macroscopic softening and liquefaction occurring at higher fluences is a gradual process, which does not produce any observable irregularity.

According to the results of optical measurements and temperature estimation, the maximum surface temperature at the ablation thresholds (0.15–0.25 J/cm^2 for the two laser temporal regimes) is between 5–15°C (the uncertainty is due to the lack of dammar's specific heat). This is in good agreement with detected phase explosion threshold whether assuming the average value (10°C/200 mJ) for the LQS_1 laser (about 0.8 J/cm^2) while that of QS laser is slightly lower (about 0.6 J/cm^2). Before trying to explain such a difference, we have to focus on an apparently major feature: in which way can the action of a rarefaction wave produce ablation of a solid material at only 10°C temperature rise?

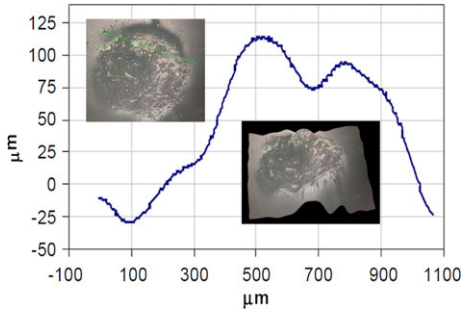

Fig. 32 Swelling of doped dammar after about 100 LQS_1 laser shot at 0.2 J/cm^2: example of 2D profile extracted from the 3D microscopy relief of the irradiated area

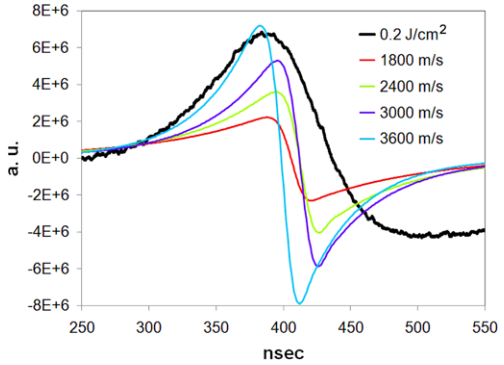

Fig. 33 Numerical simulation of photoacoustic generation produced by QS Nd:YAG laser irradiation of doped dammar at 0.2 J/cm^2

Irradiation tests at low fluence (around the ablation threshold) allowed to point out that many LQS_1 laser pulses (around 50–100) formerly produces a slight surface swelling from some tens of microns up to about 100 µm and then an irregular material detachment starts on such microprominence. Figure 32 displays an area of about 2 mm after irradiation with 100 LQS_1 laser shots at 0.22 J/cm^2, which is close to the estimated ablation threshold (Fig. 27). This phenomenon put in evidence the occurrence of under-threshold cumulative (or incubation) effects, which get important when irradiating the surface with many pulses. At higher fluences the swelling of the material is replaced by ablation.

The alteration of the material at very low fluences raises two orders of considerations. From one side it is important to investigate to which extent under-threshold cumulative effects can be exploited in combined cleaning approaches, where LQS_1 laser irradiation could be used to weaken the structure of the varnish thus allowing an easy removal using mild mechanical and/or chemical actions. On the other side, substantial insights are needed in order to gain a deeper knowledge of the phenomenon, which could be due to a superposition of contributions such as energy transfer at molecular level, action of the photomechanical wave, optical inhomogeneities of the doping, and material impurities. The latter likely play an important role also for single pulse irradiation at higher fluences. Dammar resin contains various substances exhibiting phase transitions at lower temperatures, such as for example dammar waxes [153].

The hypothesis of minor phase changes preceding the massive glass transition at 0.6–0.8 J/cm^2 could also explain the high amplitude and broadening of the compression peak observed when using the QS laser. Whereas this phenomenon could be less photomechanically pronounced for the LQS_1 Nd:YAG laser. This interpretation was also suggested by comparison of the experimental pressure transients with those provided by the 1-dimensional photoacoustic generation theory briefly summarized above.

In Fig. 33 we tried to simulate the leading edge of the profile produced by QS laser at 0.2 J/cm^2. As shown, the slope of the pressure rise is achieved, to some extent, by assuming a propagation speed of 3600 m/s. On the other hand, the calculated peak is rather narrower than the measured one. Once again, this evidences that a non-linear pressure generation was superimposed to the thermoelastic effect, which better represents the peak profile generated by LQS_1 laser (Fig. 34). The almost perfect coincidence of the calculated peak with the measured profile in the latter case was achieved by assuming a propagation speed of 1900 m/s.

The picture of laser-varnish interaction phenomena refigured above allows for formulating the following description of the ablation processes. At low fluences, the varnish is weakened by low-threshold softening processes; then the stretching phase of the photo-generated pressure transient detaches a given amount of material. This ablation channel is what was previously named *primary spallation* [44, 45].

When the stretching wave gets destructive it disappears from the pressure transient, since spallation also "interrupts" the reflection at the dammar-air interface. This is the reason why symmetric rarefaction peaks are observed only at very low fluences, whereas already at 0.2 J/cm^2 for QS and at 0.4 J/cm^2 for a LQS_1 (Fig. 29) laser it starts to be heavily attenuated because of the material spallation. Around the glass transition fluences, the pressure peaks become single-phase and that of LQS_1 also exhibit a slight broadening (from 155 to 205 ns). The latter feature suggests the occurrence of a cumulative effect given by the gradual switching toward a fluid-dynamic regime. Actually, at 0.9 J/cm^2 a similar fitting as that of Figs. 33, 34 provides a speed estimation of 3600 m/s. The broadening is less pronounced for the QS laser because, according to the previous discussion, its photomechanical generation cumulates a fluid-dynamic contribution already at low fluences.

6.1.2 Laser ablation of black crust

Pressure measurements carried out on black crust under QS laser irradiation (Fig. 30) support the qualitative descriptions of the ablation processes involved in laser cleaning of stone reported in previous works [45].

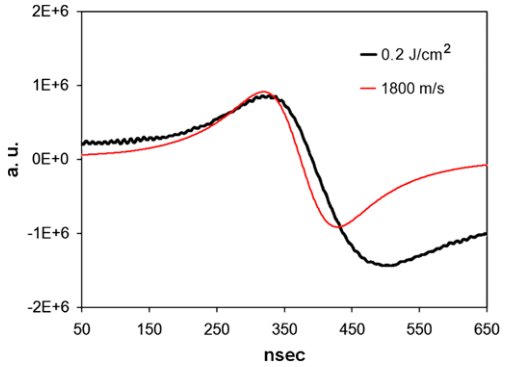

Fig. 34 Numerical simulation of photoacoustic generation by LQS_1 laser irradiation of doped dammar at 0.2 J/cm^2

Despite the discrete nature of the optical absorption, a macroscopic double-phase pulse was observed at low fluences (some hundred mJ/cm^2), which preserves only the compression phase and gets broader at high fluences.

The sound speed in the composite medium given by black crust and water assists was estimated to be about 2300 m/s. For a laser pulse width of 10 ns the corresponding propagation length is 23 μm, which is in the same order of magnitude as the measured optical penetration $\delta = 27$ μm and then laser irradiation is not inertially confined.

Laser ablation can be driven by fast thermal expansion or by vaporization of a given amount of water around absorbing centers. As a matter of fact no discontinuities were found in ablation rate curves, which suggested the vaporization was predominant since the beginning (at low fluences) but the removal was strongly assisted by photomechanical generation. An estimation of the typical radial size of the microvolume vaporized is derivable from the thermal diffusion length $l_{th} = 2(D_w \cdot t_L)^{1/2}$ (D_w: thermal diffusivity of water): 76 nm, 264 nm, 4.8–8.3 μm for QS(10 ns), LQS_1(120 ns), and SFR (40–120 μs), respectively. The comparison of operative energy densities with ε_{cr} estimated enables us to make the following considerations.

For SFR laser pulses the energy densities at the threshold are compatible with a massive vaporization of water content ($\varepsilon_w = C_w \cdot \Delta T + Q_w = 2591$ J/cm^3, with C_w at constant pressure specific heat and Q_w latent heat of vaporization of water); conversely, for QS and LQS_1 regimes one achieves a kind of paradox for the *blow-off* model used to fit the ablation rates (Figs. 2–4) since the vaporization is almost negligible. Let us consider the operative fluences: 0.8 J/cm^2 for QS(10 ns), 1.5 J/cm^2 for LQS_1(120 ns) and 7 J/cm^2 for SFR (100 μs). The corresponding energy densities for $\delta = 20$–30 μm are: 267–400 J/cm^3, 500–750 J/cm^3, 2333–3500 J/cm^3.

SFR laser energy densities are compatible with the vaporization of a relevant fraction of the water that imbibes the irradiated volume, which produces a vapor plume often noticeable to the naked eye. Conversely, the corresponding amount for short pulses (QS and LQS_1) could be almost negligible but a large increase of volume is associated with the phase explosion, because the heating is much more localized. The pressure peaks detected for the QS show the generation of a coherent macroscopic pressure transient (Fig. 30) produced by the superposition of the many microscopic sources whose stretching phase can substantially contribute to the removal process.

The width of the positive phase observed ranges between 170–300 ns, which evidences a "prolonged" compression action of the ablation plume due to the fluid-dynamic regime, which is better described by blast theory (see for example [154] and references therein). Conversely, it is not reasonable to assume an alteration of the optical penetration of a factor ten, which could alternatively explain the present duration.

Likely, also the case of the removal of calcareous stratifications on wall paintings (Figs. 20–22) involves a similar explosive vaporization of the water assists around the carbon absorbing component between crust and pictorial layer. The resulting removal process has been previously indicated as *secondary spallation* [44, 45], since it is produced by a pressure generation beneath the non-absorbing whitish crust rather than in the irradiated volume, as for *primary spallation*. However, this case needs further specific investigations also to clarify the existence and a possible role of the stretching phase. This feature will be the subject of forthcoming studies.

7 Conclusions

The things reported above aim at supporting the broadening of the application perspective of adjustable pulse duration Nd:YAG(1064) lasers. The advantages this approach provides in cleaning of stone and metal artifacts, as well as in passivating treatments of corroded bronze and iron, were shown through laboratory investigation and example applications. In this respect, insights on compositional features were achieved using portable LIPS and Raman spectroscopy, two diagnostic techniques, which are for cases of interest ready for replacing traditional invasive laboratory analyses and provide prompt compositional answers *in situ*.

Preliminary tests on the removal of biodeteriogens and graffiti from stone artifacts suggest a potential practical usefulness of Nd:YAG laser's second harmonic (532 nm) in order to address such problems. We are now performing extensive trials in restoration yards in order to verify this preliminary conclusion.

Suitable pulse duration Nd:YAG(1064) laser systems were also used for removing deposits, limewashes applied in the past, and calcareous crusts from wall paintings. In these cases, the observed behavior of the ablation thresholds of

multiple-peaks LQS laser pulse with respect to SFR laser is very interesting, since it extends the control on the photomechanical and photothermal generation during the cleaning treatment.

Finally, the preliminary results reported on samples related with the laser cleaning of easel paintings using QS and LQS_1 lasers pointed out interesting application perspectives, which motivate the need of future application tests on concrete conservation problems. The projection of the experimentation here reported toward the case of optically absorbing varnishes suggests that phase transitions and primary spallation could play a fundamental role in the ablation processes. The LQS_1 laser allows a significant reduction of the photomechanical effects with respect to the QS laser, thus favoring a higher discrimination potential of the former.

Optimized pulse duration Nd:YAG lasers represent a powerful tool in the conservation of cultural assets. While also other laser approaches are explored, including different sources and ultrashort pulses, the consolidation and extension of Nd:YAG application through systematic investigations is of crucial importance. Laser treatments in conservation will become enduring on the condition that the scientific community will be able to extend the versatility of the laser systems and support their practical employ. Frontier studies using very innovative laser sources are justified only if they stimulate and strengthen the application of sustainable technologies. Conversely, the risk to invert the route of the successful technological transfer refigured in the introduction could get concrete.

Similarly to other advanced techniques, laser treatments in conservation will have a long life only if a stable scientific presidium will be established on its application and permanent updating. Despite the many case studies of the last decade, the lack of internal competence within most of the conservation institutions represents a weak point for the consolidation of the laser methodologies. Thus, now more than ever, the state of the art provides concrete motivations for research activities aimed at assessing the correct definition of the laser treatments in restoration works, performing laboratory simulations, and basic studies on novel technologies.

Following this philosophy, we proposed here a proactive overview of the state of the art by trying to renew the interest on a set of laser cleaning aspects related with both the physical interpretation and practical application, which are still open.

Acknowledgements Laser cleaning methodologies represent a main topic of investigation of the European project CHARISMA (FP7 Capacities, Research Infrastructures, grant agreement no. 228330). At the same time, laser technologies for diagnostics and restoration of cultural assets here employed are under development within the project TEM*ART* financed by the Tuscany Region (POR-CReO/FESR 2007–2013). The present work was possible thanks to the resources provided by these two projects.

References

1. L. Lazzarini, J.F. Asmus, M. Marchesini, in *Proceedings of the 1st Int. Symp. on the Deterioration of Building Stones*, La Rochelle (1972), pp. 89–94
2. J.F. Asmus, C.G. Murphy, W.H. Munk, in *Developments in Laser Technology II*, ed. by R.F. Wuerker. Proc. SPIE, vol. 41 (1973), pp. 19–30
3. J.F. Asmus, Technol. Conserv. **3**, 14 (1978)
4. J.F. Asmus, IEEE Circuits Devices Mag. **2**, 6 (1986)
5. R. Salimbeni, R. Pini, S. Siano, G. Calcagno, J. Cult. Heritage **1**, 385 (2000)
6. A. Giusti, C. Biliotti, C. Samarelli, OPD, Restauro **8**, 120 (1996)
7. G. Orial, J.P. Gaufillet, in *Technologie Industrielle Conservation Restauration du Patrimoine Culturel, Colloque AFTPV/SFIIC*, Nice (1989), pp. 118–125
8. G. Orial, in *Preservation and Restoration of Cultural Heritage*. Proc. of the LCP Cong. (Ecole Polytechnique Fédérale de Lausanne, Lausanne, 1995), pp. 469–479
9. V. Vergès-Belmin, C. Pichot, G. Orial, in *Conservation of Stone and Other Materials*, ed. by M.J. Thiel. Proc. Int. of the RILEM/UNESCO Congress, Paris (1993), pp. 534–541
10. V. Vergès-Belmin, C. Pichot, G. Orial, in *EUROCARE-EUROMARBLE EU 496: Proceedings of the 4th Workshop*, ed. by R. Snethlage, V. Vergès-Belmin, Arles, 1993. Forschungsbericht, vol. 13 (Bayerisches Landesamt für Denkmalpflege, Munich, 1993)
11. V. Vergès-Belmin, in *Preservation and Restoration of Cultural Heritage*. Proc. of the LCP Congress (Ecole Polytechnique Fédérale de Lausanne, Lausanne, 1995), pp. 481–490
12. C. Weeks, Stud. Conserv. **43**, 101 (1998)
13. P. Bromblet, M. Labouré, G. Orial, J. Cult. Heritage **4**, 17S (2003)
14. M.I. Cooper, D.C. Emmony, J.H. Larson, in *Proceedings of the 7th International Congress on Deterioration and Cleaning of Stone*, Lisbon (1992), pp. 1305–1307
15. M.I. Cooper, D.C. Emmony, J.H. Larson, in *Proceedings of Conference on Conservation Science in the UK*, Glasgow, UK, May (1993), pp. 29–32
16. M.I. Cooper, D.C. Emmony, J. Larson, Opt. Laser Technol. **27**, 69 (1995)
17. J. Delgado Rodrigues, A.E. Charola, in *Jerónimos Monastery, the Conservation Intervention* (Cadernos IPPAR, Lisboa, 2006), pp. 199–206
18. G. Calcagno, M. Koller, Nimmrichter, Restauratoren Blätter (Special Issue: LACONA I), 39 (1997)
19. G. Calcagno, E. Pummer, M. Koller, J. Cult. Heritage **1**, S111 (2000)
20. J. Delgado Rodrigues, A. Bouineau, A. Pasetti, A.F. Belém, D. Garnier, P. Wazen, in *Atti del Convegno La pulitura delle superfici dell'architettura*, Padova (1995)
21. A. Bouineau, J. Delgado Rodrigues, A. Pasetti, in *Conservation et restauration des biens culturels: pierre, pollution atmosphérique, peinture murale, études scientifiques et cas pratiques: actes du Congrès LCP 1995*, Montreux 1995, ed. by R. Pancella (Ecole Polytechnique Fédérale de Lausanne, Lausanne, 1996), pp. 707–709
22. S. Siano, F. Margheri, P. Mazzinghi, R. Pini, R. Salimbeni, G. Toci, M. Vannini, in *Proc. Int. Conf. on LASERS 95*, Charleston, USA (1995), pp. 441–444
23. S. Siano, F. Margheri, P. Mazzinghi, R. Pini, R. Salimbeni, Appl. Opt. **36**, 7073 (1997)
24. S. Siano, F. Fabiani, R. Pini, R. Salimbeni, M. Giamello, G. Sabatini, J. Cult. Heritage **1**, S47 (2000)
25. I. Gobernado-Mitre, A.C. Prieto, V. Zafiropulos, Y. Spetsidou, C. Fotakis, Appl. Spectrosc. **51**, 1125 (1997)

26. P.V. Maravelaki, V. Zafiropulos, V. Kylikoglou, M.P. Kalaitzaki, C. Fotakis, Spectrochim. Acta B **52**, 41 (1997)
27. P.V. Maravelaki-Kalaitzaki, V. Zafiropulos, C. Fotakis, Appl. Surf. Sci. **148**, 92 (1999)
28. P. Maravelaki-Kalaitzaki, V. Zafiropulos, P. Pouli, D. Anglos, C. Balas, R. Salimbeni, S. Siano, R. Pini, J. Cult. Heritage **4**, 77s (2003)
29. S. Klein, T. Stratoudaki, V. Zafiropulos, J. Hildenhagen, K. Dickmann, T. Lehmkuhl, Appl. Phys. A **69**, 441 (1999)
30. G. Marakis, P. Maravelaki, V. Zafiropulos, S. Klein, J. Hildenhagen, K. Dickmann, J. Cult. Heritage **1**, S61 (2000)
31. G. Sabatini, M. Giamello, R. Pini, S. Siano, R. Salimbeni, J. Cult. Heritage **1**, S1 (2000)
32. M. Labouré, P. Bromblet, G. Orial, G. Wiedemann, C. Simon Boisson, J. Cult. Heritage **1**, S21 (2000)
33. R. Salimbeni, R. Pini, S. Siano, Spectrochim. Acta B **56**, 877 (2001)
34. L. Bartoli, P. Pouli, C. Fotakis, S. Siano, R. Salimbeni, Laser Chem. **2006**, 81750 (2006)
35. W. Kautek, E. Konig, C. Fotakis, V. Vergès-Belmin, K. Watkins, G. Bonsanti (eds.), *Lasers in the Conservation of Artworks: Proc. of the Int. Conf. LACONA I*, Heraklion, Crete, Greece, 4–6 October 1995 (Restauratoren Blätter, Wien, 1997) (Special Issue: LACONA I)
36. R. Salimbeni, G. Bonsanti (eds.), *Lasers in the Conservation of Artworks: Proc. of the Int. Conf. LACONA III*, Florence, Italy, 26–29 April 1999, J. Cult. Heritage **1**(1) (2000)
37. V. Verges-Belmin (ed.), *Lasers in the Conservation of Artworks: Proc. Int. Conf. LACONA IV*, Paris, France, 11–14 September 2001, J. Cult. Heritage **4**(1) (2003)
38. K. Dickmann, C. Fotakis, J.F. Asmus (eds.), *Lasers in the Conservation of Artworks: Proc. Int. Conf. LACONA V*, Osnabrück, Germany, 15–18 September 2003 (Springer, Heidelberg, 2005)
39. J. Nimmrichter, W. Kautek, M. Schreiner (eds.), *Lasers in the Conservation of Artworks: Proc. Int. Conf. LACONA VI*, Vienna, Austria, 21–25 September 2005 (Springer, Heidelberg, 2007)
40. M. Castillejo, P. Moreno, M. Oujja, R. Radvan, J. Ruiz (eds.), *Lasers in the Conservation of Artworks: Proc. Int. Conf. LACONA VII*, Madrid, Spain, 17–21 September 2007 (CRC Press, Taylor & Francis Group, London, 2008)
41. R. Radvan, J.F. Asmus, M. Castillejo, P. Pouli, A. Nevin, *Lasers in the Conservation of Artworks: Proc. Int. Conf. LACONA VIII*, Sibiu, Romania, 21–25 September 2009 (CRC Press, Taylor & Francis Group, Boca Raton, 2011)
42. M. Cooper, *Laser Cleaning in Conservation* (Butterworth Heinemann, Oxford, 1998)
43. C. Fotakis, D. Anglos, V. Zafiropulos, S. Georgiou, V. Tornari, *Lasers in the Preservation of Cultural Heritage: Principles and Applications*. Series in Optics and Optoelectronics (CRC Press, Taylor & Francis Group, Boca Raton, 2007)
44. S. Siano, in *Handbook on the Use of Lasers in Conservation and Conservation Science*, ed. by M. Schreiner, M. Strlič. http://alpha1.infim.ro/cost/pagini/handbook/chapters/prin_cle.htm
45. S. Siano, R. Salimbeni, Acc. Chem. Res. **43**, 739 (2010)
46. S. Georgiou, D. Anglos, C. Fotakis, Contemp. Phys. **49**, 1 (2008)
47. R. Pini, S. Siano, R. Salimbeni, V. Piazza, A.M. Iannucci, M. Giamello, G. Sabatini, F. Bevilacqua, J. Cult. Heritage **1**, S93 (2000)
48. M. Cooper, S. Sportun, in *LACONA VI Proc.*, ed. by J. Nimmrichter, W. Kautek, M. Schreiner (Springer, Heidelberg, 2007), pp. 55–64
49. P. Pouli, K. Frantzikinaki, E. Papakonstantinou, V. Zafiropulos, C. Fotakis, in *LACONA V Proc.*, ed. by K. Dickmann, C. Fotakis, J.F. Asmus (Springer, Heidelberg, 2005), pp. 333–340
50. A. Giusti (ed.), *Donatello restaurato*. I marmi del pulpito di Prato. (Maschietto&Musolino, Siena, 2000)
51. R. Salimbeni, R. Pini, S. Siano, in *4th EC Conf. on Research for Protection, Conservation and Enhancement of Cultural Heritage: Opportunities for European Enterprises*, Strasbourg (2000), pp. 65–73
52. S. Siano, R. Salimbeni, R. Pini, M. Matteini, S. Porcinai, A.M. Giusti, A. Casciani, J. Cult. Heritage **4**, 123s (2003)
53. M. Giamello, D. Pinna, S. Porcinai, G. Sabatini, S. Siano, in *Proc. 10th Inter. Cong. on Deterioration and Conservation of Stone*, Stockholm (2004), pp. 841–848
54. S. Siano, A. Giusti, D. Pinna, S. Porcinai, M. Giamello, G. Sabatini, R. Salimbeni, in *LACONA V Proc.*, ed. by K. Dickmann, C. Fotakis, J.F. Asmus (Springer, Berlin, 2005), pp. 171–178
55. A. Sansonetti, A. Pasetti, in *Proc. of 4th Int. Symp. on the Conservation of Monuments in the Mediterranean*, vol. 3 (1997), pp. 345–354
56. V. Vergès-Belmin, C. Dignard, J. Cul. Heritage, **4**, 238 (2003)
57. S. Klein, F. Fekrsanati, J. Hildenhagen, K. Dickmann, H. Uphoff, Y. Marakis, V. Zafiropulos, Appl. Surf. Sci. **171**, 243 (2001)
58. K. Dickmann, S. Klein, V. Zafiropulos, in *Laser Techniques and Systems in Art Conservation*, ed. by R. Salimbeni. Proc. SPIE, vol. 4402 (SPIE, Bellingham, 2001), pp. 54–67
59. P. Pouli, G. Totou, V. Zafiropulos, C. Fotakis, M. Oujja, E. Rebollar, M. Castillejo, C. Domingo, A. Laborde, in *LACONA VI Proc.*, ed. by J. Nimmrichter, W. Kautek, M. Schreiner (Springer, Heidelberg, 2007), pp. 105–114
60. S. Siano, M. Giamello, L. Bartoli, A. Mencaglia, V. Parfenov, R. Salimbeni, Laser Phys. **18**, 27 (2008)
61. F. Margheri, S. Modi, L. Masotti, P. Mazzinghi, R. Pini, S. Siano, R. Salimbeni, J. Cult. Heritage **1**, S119 (2000)
62. G. Marakis, P. Pouli, V. Zafiropoulos, P. Maravelaki-Kalaitzaki, J. Cult. Heritage **4**, S83 (2003)
63. S. Batishche, A. Englezis, T. Gorovets, A. Kouzmouk, U. Pilipenka, P. Pouli, H. Tatur, Appl. Surf. Sci. **248**, 264 (2005)
64. P. Pouli, C. Fotakis, B. Hermosin, C. Saiz-Jimenez, C. Domingo, M. Oujja, M. Castillejo, Spectrochim. Acta A **71**, 932 (2008)
65. V. Zafiropulos, P. Pouli, V. Kylikoglou, P. Maravelaki-Kalaitzaki, B.S. Lukyanchuk, A. Dogarion, in *LACONA V Proc.* (Springer, Heidelberg, 2005), pp. 311–318
66. E. Tanguy, N. Huet, Vinçotte, in *LACONA V Proc.*, ed. by K. Dickmann, C. Fotakis, J.F. Asmus (Springer, Heidelberg, 2005), pp. 125–132
67. K. Liu, E. Garmire, Appl. Opt. **34**, 4409 (1995)
68. C. Gómez, A. Costela, I. García-Moreno, R. Sastre, Appl. Surf. Sci. **252**, 2782 (2006)
69. S. Klein, T. Stratoudaki, Y. Marakis, V. Zafiropulos, K. Dickmann, Appl. Surf. Sci. **157**, 1 (2000)
70. R.M. Esbert, C.M. Grossi, A. Rojo, F.J. Alonso, M. Montoto, J. Ordaz, M.C.P. de Andres, C. Escudero, E. Barrera, Sebastian, C. Rodriguez-Navarro, K. Elert, J. Cult. Heritage **4**, s50 (2003)
71. C.M. Grossi, F.J. Alonso, R.M. Esbert, A. Rojo, Color Res. Appl. **32**, 152 (2007)
72. P. Leavengood, J. Twilley, J.F. Asmus, J. Cult. Heritage **1**, S71 (2000)
73. E. Sarantopoulou, A.C. Cefalas, in *Ultraviolet Spectroscopy and UV Lasers* (Dekker, New York, 2002), pp. 191–227
74. A. de Cruz, M.L. Wolbarsht, A. Andreotti, M.P. Colombini, D. Pinna, C.F. Culberson, Stud. Conserv. **54**, 268 (2009)
75. I. Gomoiu, R. Radvan, E. Sarantopoulou, A.C. Cefalas, in *Handbook on the Use of Lasers in Conservation and Conservation Science*, ed. by M. Schreiner, M. Strlič. http://alpha1.infim.ro/cost/pagini/handbook/index.htm
76. R. Salimbeni, R. Pini, S. Siano, J. Cult. Heritage **4**, 72s (2003)
77. K. Dörschel, G. Müller, in *Future Trend in Biomedical Applications of Lasers*. Proc. SPIE, vol. 1525 (SPIE, Bellingham, 1991), pp. 253–278
78. J. Agresti, A.A. Mencaglia, S. Siano, Anal. Bioanal. Chem. **395**, 2255 (2009)

79. S. Siano, R. Salimbeni, Stud. Conserv. **46**, 269 (2001)
80. J. Debin, L. Yi, G. Min, in *Proc. of the EEC China Workshop on Preservation of Cultural Heritages*, Xian, Shaanxi, China (1991), pp. 102–109
81. R. Pini, S. Siano, R. Salimbeni, M. Pasquinucci, M. Miccio, J. Cult. Heritage **1**, S129 (2000)
82. J. Larson, in *From Marble to Chocolate: The Conservation of Modern Sculpture*, ed. by J. Heuman. Tate Gallery Conference (Archetype Publications, London, 1995), pp. 53–58
83. C.A. Cottam, D.C. Emmony, J. Larson, S. Newman, Restauratorenblätter (Special Issue), 95 (1997)
84. S. Siano, R. Pini, S. Salimbeni, A. Giusti, M. Matteini, J. Cult. Heritage **4**, 140s (2003)
85. S. Siano, F. Grazzi, V.A. Parfenov, J. Opt. Technol. **75**, 419 (2008)
86. M. Matteini, C. Lalli, I. Tosini, A. Giusti, S. Siano, J. Cult. Heritage **4**, 147s (2003)
87. S. Siano, M. Miccio, P. Palleschi, in *Un tesoro dal mare*, ed. by A. Camilli (Bandecchi & Vivaldi, Pontedera, 2004), pp. 87–92
88. S. Siano, R. Pini, S. Salimbeni, M. Vannini, Appl. Phys. B **62**, 503 (1996)
89. P. Belluzzo, S. Siano, G. Pieri, G. Lanterna, C. Innocenti, Kermes **67/68**, 59 (2007)
90. S. Siano, A. Casciani, A. Giusti, M. Matteini, R. Pini, S. Porcinai, R. Salimbeni, J. Cult. Heritage **4**, 123s (2003)
91. S. Siano, M.L. Nicolai, S. Porcinai, in *Verrocchio's David Restored*, ed. by B. Paolozzi Strozzi et al. (Giunti, Firenze, 2003), pp. 97–108
92. S. Siano, F. Grazzi, Nuovo Cimento C **30**, 123 (2007)
93. S. Agnoletti, A. Brini, E. Formigli, S. Francolini, M. Miccio, S. Siano, OPD, Restauro **15**, 84 (2003)
94. F. Burrini, S. Gennai, in *Il ritorno d'amore: l'Attis di Donatello restaurato*, ed. by B. Paolozzi Strozzi (Museo Nazionale del Bargello, Firenze, 2005), pp. 100–116
95. M.L. Nicolai, in *Donatello, il David restaurato*, ed. by B. Paolozzi Strozzi (Giunti editore, Firenze, 2008), pp. 160–167
96. S. Agnoletti, A. Brini, E. Della Schiava, S. Gennai, A. Mignemi, N. Salvioli, D. Scapati, C. Valcepina, in *I grandi bronzi del Battistero: l'arte di Vincenzo Danti discepolo di Michelangelo*, ed. by C. Davis, B. Paolozzi Strozzi (Giunti editore, Firenze, 2008), pp. 370–381
97. M. Froidevaux, M. Cooper, P. Platt, K. Watkins, in *LACONA VII Proc.*, ed. by M. Castillejo, P. Moreno, M. Oujja, R. Radvan, J. Ruiz (CRC Press, Taylor & Francis Group, London, 2008), pp. 191–198
98. K. Dickmann, J. Hildenhagen, J. Studer, E. Müsch, in *LACONA V Proc.*, ed. by K. Dickmann, C. Fotakis, J.F. Asmus (Springer, Heidelberg, 2005), pp. 71–77
99. Y.S. Koh, I. Sarady, J. Cult. Heritage **4**, 129s (2003)
100. Y.S. Koh, Sárady, in *LACONA V Proc.*, ed. by K. Dickmann, C. Fotakis, J.F. Asmus (Springer, Heidelberg, 2005), pp. 95–100
101. P. Mottner, G. Wiedemann, G. Haber, W. Conrad, A. Gervais, in *LACONA V Proc.*, ed. by K. Dickmann, C. Fotakis, J.F. Asmus (Springer, Heidelberg, 2005), pp. 79–86
102. A. Siatou, D. Charalambous, V. Argyropoulos, P. Pouli, Laser Chem. **2006**, 85324 (2006). doi:10.1155/2006/85324
103. M. Pasquinucci, S. Bianchini, A. Facella, M. Miccio, R. Pini, S. Siano, R. Salimbeni, in *Tecniche e sistemi laser per il restauro di beni culturali*, Kermes, vol. 41 (Supplemento) (Nardini Editore, Firenze, 2000), pp. 71–104
104. D. Scapati, Due armi difensive orientali del Museo Stibbert, Diploma Thesis, OPD, Florence (2004)
105. D.A. Scott, *Copper and Bronze in Art* (Getty Publications, Los Angeles, 2002)
106. D.L.A. de Faria, S. Venancio Silva, M.T. de Oliveira, J. Raman Spectrosc. **28**, 873 (1997)
107. M.A.G. Soler, G.B. Alcantara, F.Q. Soares, W.R. Viali, P.P.C. Sartoratto, J.R.L. Fernandez, S.W. da Silva, V.K. Garg, A.C. Oliveira, P.C. Morais, Surf. Sci. **601**, 3921 (2007)
108. S. Siano, A. Brunetto, A. Mencaglia, G. Guasparri, A. Scala, F. Droghini, A. Bagnoli, in *LACONA VI Proc.*, ed. by J. Nimmrichter, W. Kautek, M. Schreiner (Springer, Heidelberg, 2007), pp. 191–201
109. S. Siano, L. Appolonia, A. Piccirillo, A. Brunetto, in *LACONA VII Proc.*, ed. by M. Castillejo, P. Moreno, M. Oujja, R. Radvan, J. Ruiz (CRC Press, Taylor & Francis Group, London, 2008), pp. 191–198
110. S. Siano, M. Mascalchi, F. Fratini, in *Il cubicolo degli apostoli, nelle catacombe romane di Santa Tecla*, ed. by B. Mazzei (Città del Vaticano, 2010), pp. 253–264
111. M.G. Patrizi, B. Mazzei, M. Mascalchi, S. Siano, in *Atti del Convegno APLAR—Applicazioni LASER nel Restauro*, ed. by A. Brunetto (Il Prato, Vicenza, 2009), pp. 73–85
112. A. Andreotti, M.P. Colombini, A. Nevin, K. Melessanaki, P. Pouli, C. Fotakis, Laser Chem. **2006**, 39046 (2006). doi:10.1155/2006/39046
113. M.C. Gaetani, U. Santamaria, The Laser Cleaning of Wall Paintings. J. Cult. Heritage **1**, S199–S207 (2000)
114. A. Andreotti, M.P. Colombini, A. Felici, A. de Cruz, G. Lanterna, M. Lanfranchi, K. Nakahara, F. Penaglia, in *LACONA VI Proc.*, ed. by J. Nimmrichter, W. Kautek, M. Schreiner (Springer, Heidelberg, 2007), pp. 203–210
115. A. Sansonetti, M. Camaiti, M. Matteini, J. Striova, E.M. Castellucci, A. Andreotti, M.P. Colombini, A. de Cruz, in *Atti del Convegno APLAR—Applicazioni LASER nel Restauro*, ed. by A. Brunetto (Il Prato, Vicenza, 2009), pp. 201–210
116. J. Hildenhagen, M. Chappé, K. Dickmann, in *LACONA V Proc*, ed. by K. Dickmann, C. Fotakis, J.F. Asmus (Springer, Heidelberg, 2005), pp. 297–301
117. C.J. Herringham, *The Book of the Art of Cennino Cennini* (George Allen & Unwin, London, 1922)
118. L. Carlyle, Laser interactions with paintings: results and proposals for further study, Internal Report, The Canadian Conservation Institute, Ottawa, Canada, 1981
119. M.L. Wolbarsht, A. de Cruz, US Patent, 5,951,778 (1990)
120. E.I. Hontzopoulos, C. Fotakis, M. Doulgeridis, in *Proc. of 9th Int. Symp. on Gas Flow and Chemical Lasers*, ed. by C. Fotakis, C. Kalpouzos, T.G. Papazoglou. Proc. SPIE, vol. 1810 (SPIE, Bellingham, 1993), pp. 748–751
121. I. Zergiotti, A. Petralis, V. Zafiropulos, C. Fotakis, A. Fostiridou, M. Doulgeridis, Restauratorenblatter, Special issue (LACONA I), 57 (1997)
122. R. Salimbeni, P. Mazzinghi, R. Pini, S. Siano, M. Vannini, M. Matteini, A. Aldrovandi, in *Proc. of the 1st Int. Cong. on Science and Technology for the Safeguard of Cultural Heritage in the Mediterranean Basin*, ed. by A. Guarino. Catania, Italy, 1995 (CNR, Roma, 1998), pp. 811–815
123. S. Georgiou, V. Zafiropulos, V. Tornari, C. Fotakis, Laser Phys. **8**, 307 (1998)
124. J.H. Scholten, J.M. Teule, V. Zafiropulos, R.M.A. Heeren, J. Cult. Heritage **1**, S215 (2000)
125. R. Teule, H. Scholten, O.F. van den Brink, R.M.A. Heeren, R. Hesterman, U. Ullenius, I. Larsson, V. Zafiropulos, M. Castillejo, M. Martin, F. Guerra-Librero, A. Silva, H. Gouveia, M.B. Albuquerque, J. Cult. Heritage **4**, S209 (2003)
126. C. Theodorakopoulos, V. Zafiropulos, J. Cult. Heritage **4**, S216 (2003)
127. A. de Cruz, M.L. Wolbarsht, S.A. Hauger, J. Cult. Heritage **1**, S173 (2000)
128. P. Bracco, G. Lanterna, M. Matteini, K. Nakahara, O. Sartiani, A. de Cruz, M.L. Wolbarsht, E. Adamkiewicz, M.P. Colombini, J. Cult. Heritage **4**, 202s (2003)

129. A. Andreotti, P. Bracco, M.P. Colombini, A. de Cruz, G. Lanterna, K. Nakahara, F. Penaglia, in *LACONA VI Proc.*, ed. by W. Kautek, J. Nimmrichter, M. Schreiner (Springer, Heidelberg, 2007), pp. 239–247
130. A. Sansonetti, M. Realini, J. Cult. Heritage **1**, S189 (2000)
131. P. Pouli, D.C. Emmony, C.E. Madden, I. Sutherland, J. Cult. Heritage **4**, 271s (2003)
132. A. Schnell, L. Goretzki, Ch. Caps, in *LACONA V Proc.*, ed. by K. Dickmann, C. Fotakis, J.F. Asmus (Springer, Heidelberg, 2005), pp. 292–296
133. P. Pouli, G. Bounos, S. Georgiou, C. Fotakis, in *LACONA VI Proc.*, ed. by J. Nimmrichter, W. Kautek, M. Schreiner (Springer, Heidelberg, 2007), pp. 287–294
134. P. Pouli, I.-A. Paun, G. Bounos, S. Georgiou, C. Fotakis, Appl. Surf. Sci. **254**, 6875 (2008)
135. P. Pouli, A. Nevin, A. Andreotti, P. Colombini, C. Fotakis, Appl. Surf. Sci. **255**, 4955 (2009)
136. P. Pouli, A. Selimis, S. Georgiou, C. Fotakis, Acc. Chem. Res. **43**, 771 (2010)
137. A. Athanassiou, M. Lassithiotaki, D. Anglos, S. Georgiou, C. Fotakis, Appl. Surf. Sci. **154/155**, 89 (2000)
138. M. Lassithiotaki, A. Athanassiou, D. Anglos, S. Georgiou, C. Fotakis, Appl. Phys. A **69**, 363 (1999)
139. P. Vounisiou, A. Selimis, G.J. Tserevelakis, K. Melessanaki, P. Pouli, G. Filippidis, C. Beltsios, S. Georgiou, C. Fotakis, Appl. Phys. A **100**, 647–652 (2010)
140. A. Selimis, P. Vounisiou, G.J. Tserevelakis, K. Melessanaki, P. Pouli, G. Filippidis, C. Beltsios, S. Georgiou, C. Fotakis, Proc. SPIE **7391**, 73910U (2009). doi:10.1117/12.827658
141. K. Melessanaki, C. Stringari, C. Fotakis, D. Anglos, Laser Chem. **2006**, 42709 (2006). doi:10.1155/2006/42709
142. P. Pouli, A. Nevin, A. Andreotti, P. Colombini, S. Georgiou, C. Fotakis, Appl. Surf. Sci. **255**, 4955 (2009)
143. M. Oujja, P. Pouli, C. Domingo, C. Fotakis, M. Castillejo, Appl. Spectrosc. **64**, 528 (2010)
144. M. Oujja, A. García, C. Romero, J.R. Vázquez de Aldana, P. Moreno, M. Castillejo, Phys. Chem. Chem. Phys. **13**, 4625 (2011)
145. M. Camaiti, M. Matteini, A. Sansonetti, J. Striova, E. Castellucci, A. Andreotti, M.P. Colombini, A. de Cruz, R. Palmer, in *LACONA VII Proc.*, ed. by M. Castillejo, P. Moreno, M. Oujja, R. Radvan, J. Ruiz (CRC Press, Taylot & Francis Group, London, 2008), pp. 253–260
146. A. Ishimaru, *Wave Propagation and Scattering in Random Media* (Academic Press, New York, 1978)
147. W.-F. Cheong, A. Prahl, A.J. Welch, IEEE J. Quantum Electron. **26**, 2166 (1990)
148. L.V. Burmistrova, A.A. Karabutov, A.I. Portnyagin, O.V. Rudenko, E.B. Cherepetskaya, Sov. Phys. Acoust. **24**, 369 (1978)
149. A.A. Karabutov, O.V. Rudenko, E.B. Cherepetskaya, Sov. Phys. Acoust. **25**, 218 (1979)
150. M.W. Sigrist, J. Appl. Phys. **60**, R83 (1986)
151. R.O. Esenaliev, A.A. Oraevsky, V.S. Letokhov, A.A. Karabutov, T.V. Malinsky, Lasers Surg. Med. **13**, 470–484 (1993)
152. S. Siano, R. Pini, F. Rossi, P.G. Gobbi, R. Salimbeni, Appl. Phys. Lett. **72**, 647 (1998)
153. C.V. Horie, *Materials for Conservation* (Butterwhorths, London, 1987)
154. S. Siano, R. Pini, R. Salimbeni, Appl. Phys. Lett. **74**, 1233 (1999)